University of South Bohemia in České Budějovice, Faculty of Science,
Institute of Chemistry and Biochemistry

Insights into the Evolutionary Conserved Mitochondrial Contact Site and Cristae Organization System in Trypanosoma brucei Through RNA Interference

Bachelor of Science Thesis

Lawrence Rudy Cadena III

Supervisor: Hassan Hashimi Ph.D.

Co-Supervisor: Iosif Kaurov M.Sc.

Institute of Parasitology, Biology Center, Academy of Sciences of Czech Republic
Faculty of Science, University of South Bohemia

České Budějovice 2018

This thesis should be cited as:
Cadena L.R. (2018) Insights into the Evolutionary Conserved Mitochondrial Contact Site and Cristae Organization System in Trypanosoma brucei Through RNA Interference.

Annotation
This work aims to give insight into the evolution of the mitochondria by investigating novel properties of the evolutionary conserved mitochondrial contact site and cristae organization system complex within the Excavata clade using *Trypanosoma brucei* as our model. This study shows that this complex indeed contains diverse properties that are not present in the typically studied Opisthokonta clade: *e.g.* mammalian and yeast organisms.

Declaration [In Czech and English]

Prohlašuji, že svoji disertační práci jsem vypracovala samostatně pouze s použitím pramenů a literatury uvedených v seznamu citované Iteratury. Prohlašuji, že v souladu s § 47b zákona č. 111/1998 Sb. v platném znění souhlasím sezveřejněním své disertační práce, a to v úpravě vzniklé vypuštěním vyznačených částí archivovaných Přírodovědeckou fakultou elektronicko u cestou ve veřejně přístupnéčásti databáze STAG provozované Jihočeskou univerzitou v Českých Budějovicích na jejích internetových stránkách, a to se zachováním mého autorského práva k odevzdanému textu této kvalifikační práce. Souhlasím dále s tím, aby toutéž elektronickou cestou byly v souladu s uvedeným usta novením zákona č. 111/1998 Sb. zveřejněny posudky školitele a oponentů práce i záz nam o průběhu a výsledku obhajoby kvalifikační práce. Rovněž souhlasím s por ovnáním textu mé kvalifikační práce s databází kvalifikačních prací Theses.cz pro vozovanou Národním registrem vysokoškolských kvalifikačních prací a systémem na odhalování plagiátů.

I hereby declare that, in accordance with Article 47b of Act No. 111/1998 in the valid wording, I agree with the publication of my thesis, in full to be kept in the Faculty of Science archive, in electronic form in publicly accessible part of STAG database operated by the University of South Bohemia in České Budějovice accessible through its web pages. Further, I agree to the electronic publication of the comments of my supervisor and thesis opponents and the record of the proceedings and results of the thesis defence in accordance with aforementioned Act. No. 111/1998. I also agree to the comparison of the text of my thesis with the Thesis.cz thesis database operated by the National Registry of University and a plagiarism detection system.

České Budějovice,.....

……
Lawrence Rudy Cadena III

Financial Support

Support from the Czech Grant Agency 17-24036S

Acknowledgements [In English and Ukrainian]

I'm not usually very good at this sort of thing, but I guess I'll start where it feels right. I reckon I wouldn't have imagined I'd be in the situation where I currently am two years ago when I first walked into this lab. It's kinda funny how looking back on things it seems like a hell of a lot has happened since then, and it has… These past two years left quite an impression on me. So I'd like to start off with acknowledging seven special individuals who indeed changed a few paths in my life for the better, all without the constraints of academic formality.

I've gotta tell you Hassan Hashimi, it was pretty much pure luck I ended up talking to you that October afternoon. First few months I had a bit of doubts on how things were going. But with time we started getting pretty good results and it was that motivation that kept the ball rollin' for me. You're a pretty good leader, and that's somewhat hard to find nowadays. You also opened a few doors for me that honestly you didn't have to, but that just made my interest in this work grow more. I'd like to thank you for everything you've done that got me here today. And even though we had our disagreements, you're reasoning behind them made sense with time. I hope we'll be able to work on a lot of neat projects in the future together, I've gotta feeling we'll make a pretty good team.

Iosif Kaurov, thanks a bunch for the help, especially the first few months where I had no clue what to do. You're a pretty cool guy and great to work with. I know that we'll end up working on future projects together and end up late night drinking again soon when I'm back in Budejovice. I'm pretty glad we were able to move from lab partners to friends.

Julius (Jula) Lukeš, you're a unique fella, and I'd like to thank you for giving me the opportunity to work in the field of parasitology. As well as giving me the chance to party at conferences, hopefully I'll end up being more useful to you in these sorts of things soon.

I'd also like to extend my thanks to Jirka Heller for all the technical help and kindness he's shown during my time in the lab, looking forward to working with you soon again.

And to the very special gal who is an important part of both my academic and personal life, I wish to extend my ever grateful thanks to my best friend, Daria Tashyreva, for her friendship and support throughout my time in Budejovice and abroad. *Дарія моя найдорожча маленька "gal" дякую тобі за все.Ти була, та все ще є, моєю найбільшою емоційною підтримкою. І, найважливіше, моїм кращим другом. Сподіваюсь що ти знаєш яке важливе місце ти займаєш в моєму серці, і я з нетерпінням чекаю що для нас готує майбутнє. Дякую*

And one final show of gratitude to my friends in Linz & Budejovice (you know who you are) and to my close family, especially my father and mother. Thank you dad, for your support and believing in me since the start of my journey. I seriously doubt I would have been able to make it without you and mom. Finally, someone in the family who won't end up becoming a lawyer, right? Hope I made you two proud here. Thank you for everything and for all the hardship you endured to give me a good chance at life.

Here's to many more to come, Na zdraví!

List of author's contributions and conference presentations

The thesis is based on the following works (listed chronologically):

I. **Cadena, L.R.**, Kaurov, I., Lukeš, J., Hashimi, H., (2017) The application of Gibson Assembly to steamline generation of long hairpin RNAi constructs for inducible knockdown of MICOS subunits in Trypanosoma brucei. *47th Jirovec's Protozoological Days*

II. **Cadena, L.R.**, Kaurov, I., Lukeš, J., Hashimi, H., (2018) Dropping the Mic: Knockdown of MICOS subunits yields an intriguing phenomenon in Trypanosoma brucei. *48th Jirovec's Protozoological Days*

III. Kaurov, I., Vancová, M., Schimanski, B., **Cadena, L.R.**, Heller, J., Bílý, T., Potěšil, T., Eichenberger, C., Bruce, H., Oeljeklaus, S., Warscheid, B., Zdráhal, Z., Schneider, A., Lukeš, J., Hashimi, H., (2018) Diverged Trypanosome MICOS as a Hub for Mitochondrial Cristae Shaping and Protein Import. *Manuscript in submission*

Lawrence Cadena performed the following laboratory experiments: Establishment of a pipeline for Gibson Cloning, cell line generation, growth analysis, immunoblot analysis and sample preparation for transmission electron microscopy

Table of Contents

1. Abstract

Cristae are infolded sub-compartments of the inner membrane of the mitochondrion, giving the organelle its distinctive morphology and increase in surface area to allow greater capacity for adenosine triphosphate generation via respiratory chain complexes that perform oxidative phosphorylation. In order to achieve proper cristae morphology, cooperation among cristae-shaping proteins is needed. The mitochondrial contact site and cristae organization system (MICOS) is a one protein complex that fulfills this role. In studied organisms thus far, it is located at cristae junctions, narrow neck-like structures that connect cristae to the inner membrane. The majority of what we know about this complex is limited to opisthokont models (*e.g.* humans) yielding little information about other potential properties of this complex that may have evolved in other eukaryotes. As a eukaryote with a long independent evolutionary history, *Trypanosoma brucei* (Tb) plays a beneficial role in understanding the evolutionary divergence of mitochondria. Here we investigate the proteins that co-immunoprecipitate with the sole recognizable MICOS subunit found in *T. brucei* genome: the paralogs TbMic10-1 and TbMic10-2. Knockdown of these individual proteins via RNA interference results not only in cellular growth arrest and altered cristae morphology, but also in the downregulation TbMic10-1, supporting the idea that these proteins are components of a novel TbMICOS complex. Surprisingly, knockdown of certain putative subunits results in the downregulation of an essential pathway protein needed in the biogenesis of small precursor intermembrane space proteins. This result is the possible identification of the central enzyme, a MICOS subunit, which is responsible for the importation of small cysteine-containing proteins into the intermembrane space. This is an intriguing phenomenon, as a functional homolog for this central enzyme has previously been postulated to be absent in *Trypanosoma brucei*.

2. Aims and Tasks

The aim of this research was to:

I. create constructs for RNA interference (RNAi) to knockdown proteins that co-immunoprecipitate with the evolutionary conserved TbMIC10-1/2 paralogs in *Trypanosoma brucei*;
II. establish the pipeline for the Gibson Assembly molecular cloning method to mediate constructs for RNAi in *Trypanosoma brucei*;
III. investigate whether knockdown of individual putative TbMICOS subunits would alter cell fitness;
IV. investigate the effects on cristae morphology after knockdown of individual putative TbMICOS subunits based on transmission electron microscopy images;
V. investigate the effects on TbMIC10-1 expression levels after knockdown of individual putative TbMICOS subunits;
VI. investigate whether knockdown of individual putative TbMICOS subunits downregulate or upregulate any key mitochondrial proteins.

3. Introduction

3.1. Trypanosoma brucei

Trypanosomes are unicellular parasitic protozoa belonging to the class Kinetoplastea, part of the much larger excavata supergroup. Given the Kinetoplastea position on the Eukaryote tree of life and extended evolutionary distance, Trypanosoma provides an excellent organism for the study of cellular diversity (Figure 1) (Hampl et al., 2009).

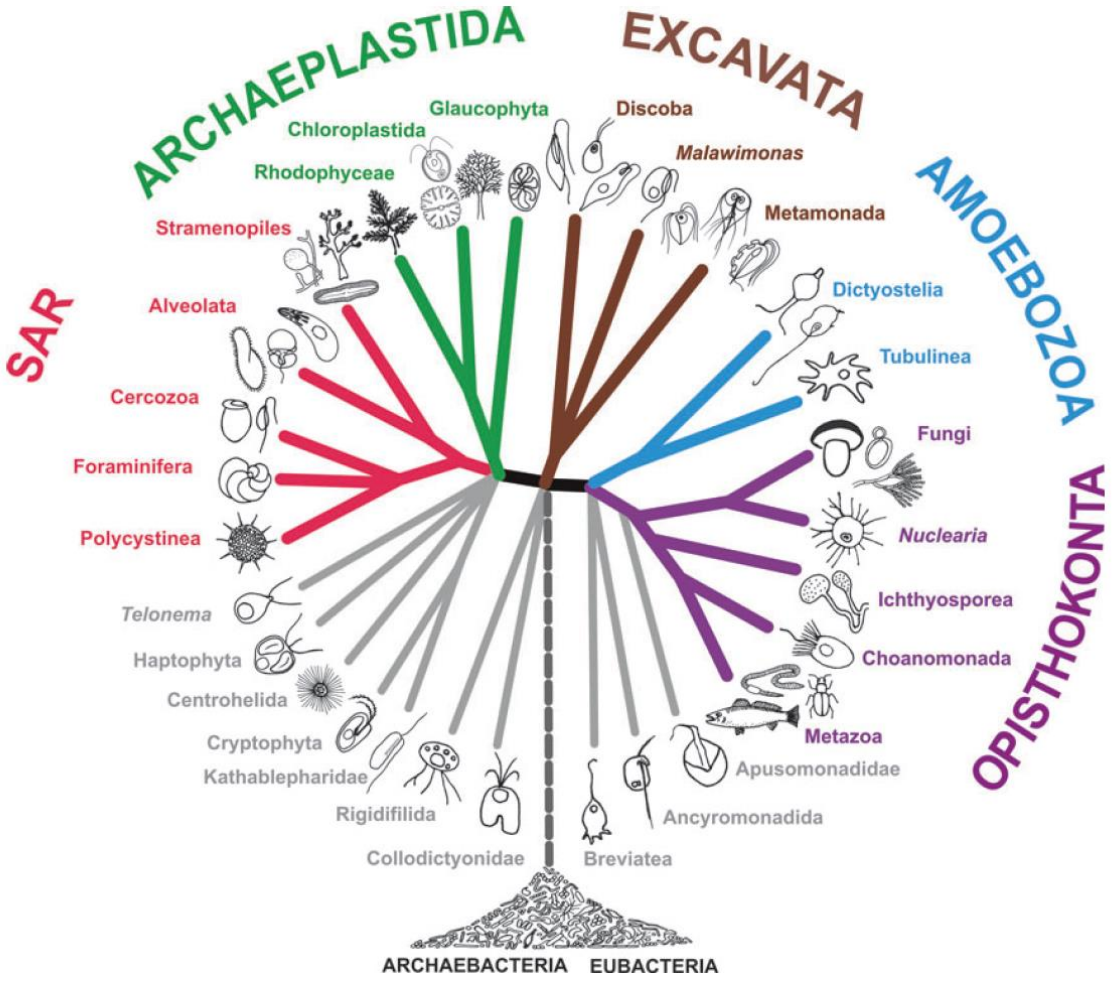

Fig.1. Revised phylogeny classification of eukaryotes. Trypanosomes fall under the Discoba clade. Source: Adl et al., 2012

A species of trypanosomes, *Trypanosoma brucei*, is an ideal experimental model organism for the study of various aspects of cell biology (Matthews 2005). This is in part due to the nature of this exotic organism. As a heteroxenous parasite, *T. brucei* has many distinct stages in its life cycle in order to adapt to various diverse environments containing different nutrients. Within the mammalian hosts, *T. brucei* contains two major forms, the short-stumpy and the long-slender bloodstream forms. While three major forms are found in different portions of the insect vector: the procyclic form located within the midgut, and the epimastigote and metacyclic trypomastigotes in the salivary glands (Vickerman 1985).

T. brucei contains a single mitochondrion that undergoes major remodeling throughout its life cycle (Zikova et al., 2017). During the procyclic cycle it contains a classical mitochondrion with abundant cristae and the capacity for oxidative phosphorylation (OXPHOS), a metabolic pathway in which nutrients are oxidized to release energy for the production of adenosine triphosphate. However during the bloodstream cycle both cristae and OXPHOS disappear, along with the reduction in the overall size of the mitochondrion (Jakob 2016; Vickerman 1965).

3.2. RNA Interference

RNA interference (RNAi) is a regulatory pathway in which small double-stranded RNA (dsRNA) molecules inhibit gene expression via silencing of targeted mRNA molecules (Fire et al., 1998). This pathway is found in many eukaryotes, using the Dicer enzyme to cleave long dsRNA into shorter dsRNA known as small interfering RNA (siRNA). The siRNA separates into two single stranded RNA (ssRNA), known as the passenger strand and the guide strand, with the former being degraded in the process. The guide strand is left to incorporate itself into the RNA-induce silencing complex (RISC), resulting in post-transcriptional gene silencing by forming complimentary sequences with mRNA, rendering it degraded (Figure 2).

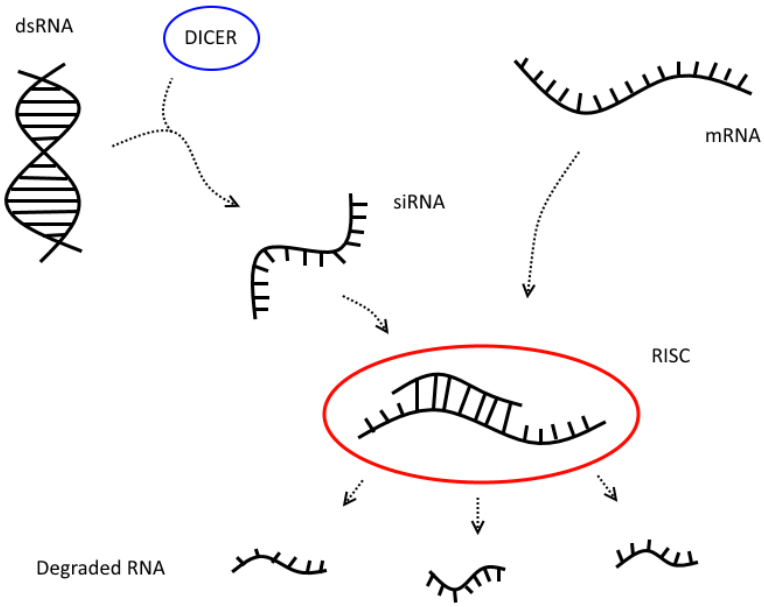

Fig.2. Schematic showing RNA interference pathway. The Dicer enzyme cleaves to dsRNA yielding siRNA. Targeted mRNA and siRNA are then incorporated into the RISC multiprotein complex where Argonaute activates and cleaves the mRNA.

First discovered in *C. elegans* (Fire et al., 1998), RNAi was also independently discovered in *T. brucei* in the same year (Ngô et al,. 1998), though not acknowledged by the Nobel Prize committee. Unlike most other Kinetoplastida parasites, *T. brucei* retained the molecular machinery needed for RNAi, allowing transgenic manipulation to study loss of function (Ullu et al., 2012). Knockdown of our genes of interest were done based on conditional RNAi, in which the vector synthesizes dsRNA in vivo using a T7 promoter and tetracycline-inducible system to allow the inducible activation or deactivation of transcription (McAllaster et al., 2016; Wang et al., 2000; Wirtz et al., 1995). T7

polymerase is promoter-specific, allowing effective transcription downstream of the T7 promoter. The tetracycline-inducible system works by use of Tet Repressor proteins fused with the activation domain of the VP16 protein (found in the Herpes Simplex Virus) to yield Tetracycline Transactivator proteins. This protein then binds to DNA at specific tetO operator sequences only in the presents of tetracycline, allowing transcription initiation of the intendent genetic product (Gossen et al., 1995).

There are two varieties that RNAi can be triggered experimentally in *T. brucei*: constructs that employ either a dual promoter system or long hairpin RNA (lhRNA) expression. The latter results in structures in which adjacent segments of RNA fold together and are stabilized by base pairing, creating a loop of single-stranded RNA, resulting in the 'knockdown' of the targeted gene (Paddison et al., 2002). The use of long hairpin loop RNAi in comparison to dual promoters is favored largely due to decreased levels of background expression of double stranded RNA and improved base pairing in *T. brucei* (Atayde et al., 2012).

3.3. Gibson Assembly

Although *T. brucei* is known for its robust and easy molecular manipulation, one major task faced in the following investigation is the rapid assembly of long hairpin constructs for RNAi knockdowns. The most troublesome issue is the ligation of multiple DNA fragments into a single vector, although possible via conventional molecular cloning, the following method greatly shortens the time needed to generate these constructs. The introduction of multiple DNA fragments into the pTrypSon vector (see 4.1.1.) is mediated here by a molecular cloning technique known as Gibson Assembly.

Unlike conventional molecular cloning, Gibson Assembly allows rapid ligation of multiple DNA fragments with overlapping termini in a single-tube isothermal reaction, thus increasing the speed of molecular cloning (Gibson et al., 2009). This method consists of a three central enzyme cocktail (Figure 3): a 5'→3' exonuclease that chews back the overhanging sequences via a hydrolyzing reaction to allow the subsequent annealment of complimentary DNA segments. DNA polymerase to fill in the overhangs and DNA ligase to facilitate the linking of DNA strands together. The exonuclease is heat-labile and inactivated during the 50 °C incubation, thus it will not compete with the polymerase activity at this temperature. This method allows all enzymes to perform simultaneously in a single isothermal reaction. DNA fragments can be created using either restriction digest or non-annealing overhangs in PCR primers.

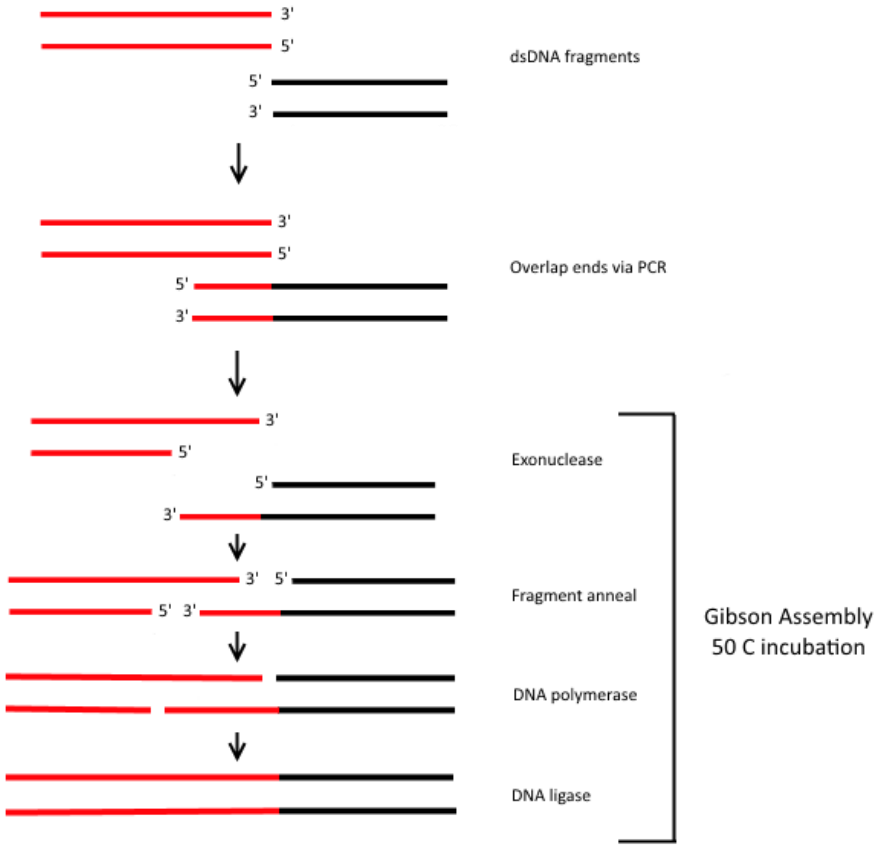

Fig.3. Schematic of the Gibson Assembly process. dsDNA fragments are inserted into a single-tube containing a multi enzyme cocktail containing exonuclease, DNA polymerase and DNA ligase to generate the final product.

3.4. The Mitochondrial Contact Site and Cristae Organization System

Mitochondrial cristae are invagnations of the mitochondrial inner membrane (MIM), providing increases in surface area to allow greater capacity for adenosine triphosphate (ATP) generation by respiratory chain complexes that perform oxidative phosphorylation (Davies et al., 2012; Vogel et al., 2006). Not only are cristae distributed throughout most eukaryotes, but they appear in diverse morphologies (Figure 4), with lamellar-shaped cristae being observed in the opisthokonta supergroup (containing animals and fungi) and discoid ‘paddle-shaped’ cristae found in most members of the excavata supergroup (Munoz-Gomez et al., 2015a). This discoid morphology currently defines the Discoba clade in excavates (Figure 1) (Adl et al., 2012).

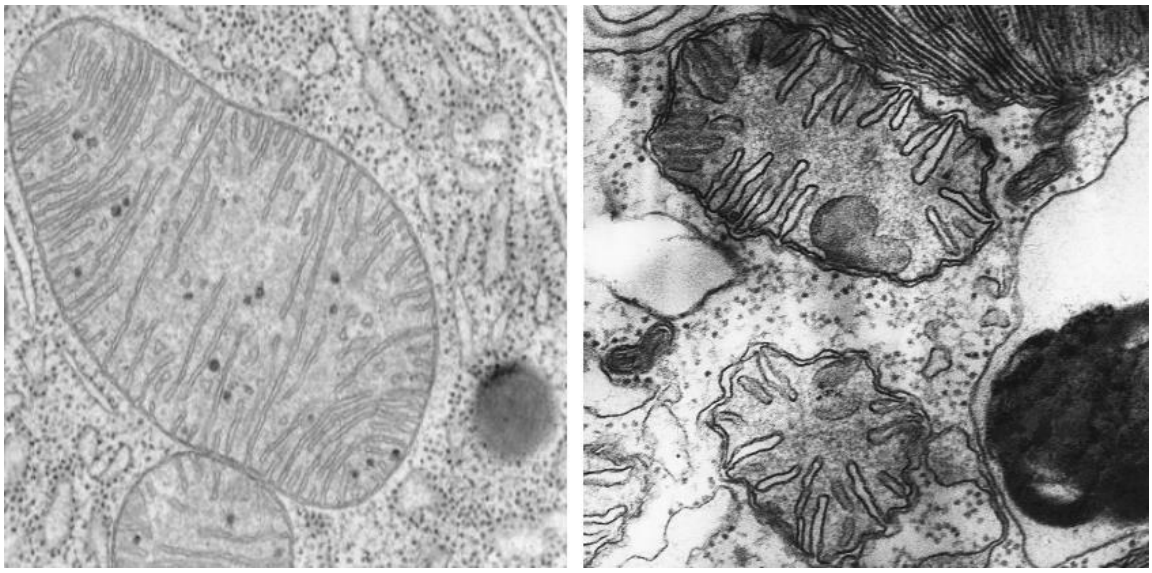

Fig.4. Transmission electron microscopy images of mitochondria showing different cristae morphologies. Flat lamellar cristae as seen in mammalian pancreatic cells (left) and discoid cristae in euglena (right). Source: Porter, K., Bonneville, M., (2011) and Biophoto Associates, respectively.

The human mitochondrial contact site and cristae organization system (MICOS) is a multiprotein complex located at cristae junctions (CJs), narrow neck-like structures that connect cristae to the inner membrane (Kozjak-Pavlovic, 2016; Rampelt et al., 2017a; Wollweber et al., 2017, Harner 2011; von der Malsburg et al., 2011; Hoppins et al., 2011). MICOS proteins are associated with the formation and maintenance of cristae, as the presence of MICOS genes in genomes correlates with the occurrence of cristae. This complex has been shown to be crucial for the biogenesis of the mitochondria due to its role in the tethering of the inner membrane and outer membrane (core subunit Mic60), as well as the controlled stabilization of cristae development through induced negative membrane curvature at CJs (core subunits Mic10 & Mic60) (Harner et al., 2011; Tarasenko et al., 2017). Opisthokonts typically contain 6-7 subunits that constitute the complex, with the deletion of core subunits Mic60 and Mic10 resulting in more severe growth defects and morphological damage than deletion of other subunits (Munoz-Gomez et al., 2015a; Ott et al., 2015). This indicates that MICOS subunits form a hierarchy in the complex based on their importance in maintaining correct cristae morphology and stability with other mitochondrial components (Friedman et al., 2015; Ott et al., 2015).

The MICOS complex does not only appear to assist with the formation of membrane curvatures at CJs (Tarasenko et al., 2017), but also interacts with other proteins embedded in the mitochondrial outer membrane (MOM), specifically the β-barrel sorting and assembly subunit (Sam50) and the multiprotein translocase of the outer membrane (TOM) (Bohnert et al., 2012; Körner et al., 2012), both part of the mitochondrial protein import machinery (Figure 5) (Wiedemann and Pfanner, 2017). To conclude, the function of MICOS is not only to provide the structural integrity of cristae, but also to mediate stable interactions with mitochondrial import complexes (Friedman et al., 2015; Horvath et al., 2015).

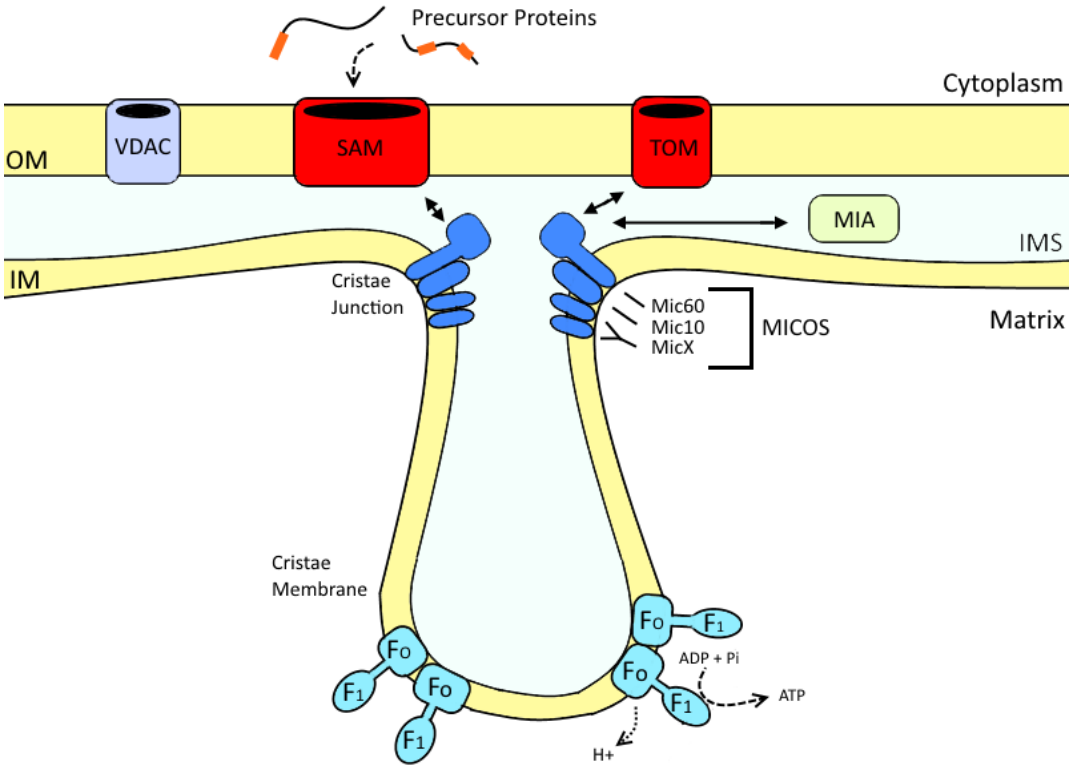

Fig.5. General depiction of MICOS in Opisthokonta, with Mic10 and Mic60 being the most conserved subunits throughout the eukaryotes and MicX being any of the other 6-7 subunits present in Opisthokont. MICOS is known to interact with Sam50, TOM and MIA proteins.

3.5. The Mitochondrial Contact Site and Cristae Organization System in *Trypanosoma*

Although the majority of MICOS components contain homologs throughout opisthokonts, only Mic10 and Mic60 seem to be present throughout most of the eukaryotes, with the former being the most widespread and the latter being the oldest (Munoz-Gomez et al., 2015a; Huynen et al., 2016). The antiquity of Mic60 is support by its presence in α-proteobacteria, being the sole MICOS component found outside eukaryotes, corroborating the endosymbiotic origin of the mitochondria from prokaryotes (Munoz-Gomez et al., 2015a). Knowledge of MICOS is limited to opisthokont models, with the Mic10 paralogs (named: TbMic10-1 and TbMic10-2) being the only MICOS components bioinformatically identified in the *T. brucei* genome (Munoz-Gomez et al., 2015b). The lack of a Mic60 homolog also suggests that *T. brucei* may contain a divergent MICOS complex with novel subunits.

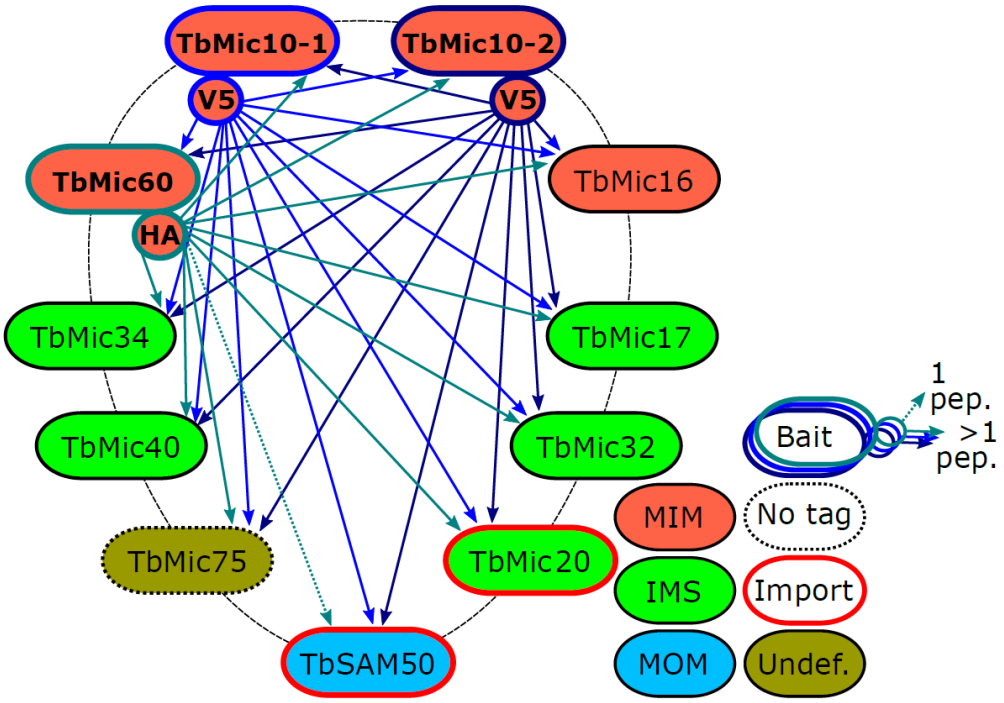

Fig.6. Immunoprecipitation map of baited TbMic10-1, TbMic10-2 and TbMic60. Nine proteins are shown to co-immunoprecipitate with TbMic10-1/2 based on Mass Spectroscopy. Proteins are named using the established MICOS nomenclature (Table 1). Localization of proteins are shown as MIM (mitochondrial inner membrane), IMS (mitochondrial inter membrane space) and MOM (mitochondrial outer membrane). TbSam50 and TbMic20 are import proteins (see results and discussion). TbMic75 also co-immunoprecipitates with the TbMic10 paralogs, however this putative subunit was not investigated due to our inability to *in situ* tag this protein, as of now it remains undefined (Kaurov et al., submitted).

Immunoprecipitation (IP) of TbMic10-1/2 shows that TbMICOS contains 9 to 11 proteins that stably interact with Mic10 paralogs (Figure 6) (Kaurov et al., submitted). Eight proteins, plus interaction partner Sam50, were subsequently chosen for further experimentation to identify their roles in cristae biogenesis, on which this thesis is based. All proteins here are named using the established MICOS nomenclature (Pfanner et al., 2014). Sam50, which is not a part of the MICOS complex, is nevertheless included in this analysis due to its co-immunoprecipitation with TbMic10 paralogs.

3.6. ERV1 and MIA40

Within the mitochondrial intermembrane space (IMS) numerous disulfide bond containing proteins exist. These cysteine-rich proteins possess a conserved twin CX_3C motif or twin CX_9C motif (Hell 2008; Stojanovski et al., 2012). In order to facilitate the introduction of disulfide bonds in precursor IMS proteins, a pathway known as the mitochondrial IMS import and assembly (MIA) pathway has been shown to rely on a disulfide relay system between two essential proteins: the sulfhydryl oxidase Erv1 and the redox-regulated import receptor Mia40 (formally known as Tim40) (Figure 7) (Hell 2008). As the central catalysis of the MIA pathway, Mia40 enables C_x3,9C motif folding via its reactive CPC motif by forming a disulfide bond with one of the thiol groups of a reduced IMS

precursor in its unfolded state (Banci et al., 2009). Erv1 mediates the oxidation of Mia40 by reoxidation of the CPC motif in Mia40, allowing the process to repeat. Since folded proteins cannot transport through TOM in the outer membrane, the substrates become trapped in the IMS, allowing the net import of proteins into the mitochondria by the MIA pathway (Hell 2008).

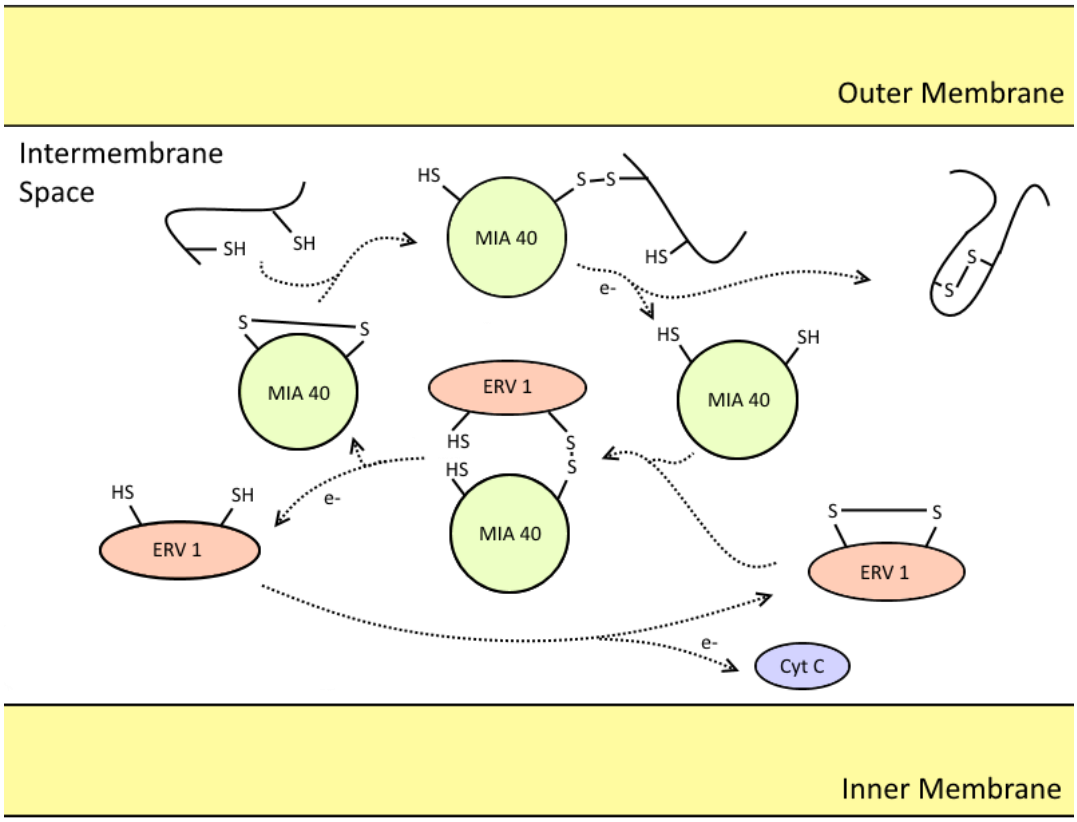

Fig.7. Simplified model of the MIA pathway as described in humans. Unfolded proteins are introduced into the IMS via TOM40 (not shown) where disulfide bonds are inserted to the precursor protein via disulfide isomerization with Mia40, leaving Mia40 in the reduced state. Erv1 has been suggested to recycle Mia40 through a reoxidation process. The now oxidized Erv1 is regenerated by transferring electrons to cytochrome *c*, where the electrons are then transported to the final electron acceptor, oxygen, under aerobic conditions (not shown).

Although there is a lack of component homology, the MIA pathway shows remarkable similarity with oxidation systems in the periplasm of bacteria, possibly reflecting the evolutionary origin of the intermembrane space with bacterial periplasm (Hell 2008). Currently there is no recognizable homolog for Mia40 in *T. brucei* (Haindrich et al., 2017), although an orthologue for Erv1 has been identified and characterized (Basu et al., 2012; Eckers et al., 2012). There is evidence that Mic60 tethers Mia40 to a subpopulation of the TOM complex in the MOM, providing evidence for an interaction between MICOS and the MIA pathway (von der Malsburg et al., 2011; Herrmann, 2011).

4. Experimental Procedures

4.1. Design of Constructs

4.1.1. pTrypSon

Due to previous studies applying RNAi in *T. brucei*, we utilized the established pTrypSon as our vector of choice for MICOS RNAi knockdowns (McAllaster et al., 2016). pTrypSon contains what is known as 'Gateway Att' sites, allowing efficient inclusion of inverted DNA segment repeats of the targeted sequence on both sides of a 'stuffer' sequence to provide a hairpin loop (Kalidas et al., 2011; Atayde et al., 2012). The region between these 'Gateway' sites can be excised by HindIII and XhoI restriction enzymes (Figure 8), allowing the insertion of any sequence of choice. The pTrypSon backbone contains an ampicillin resistance marker to allow growth and selection in *E. coli* and a NotI cleavage site for linearization near the flanks of homology to provide recombination into *T. brucei*.

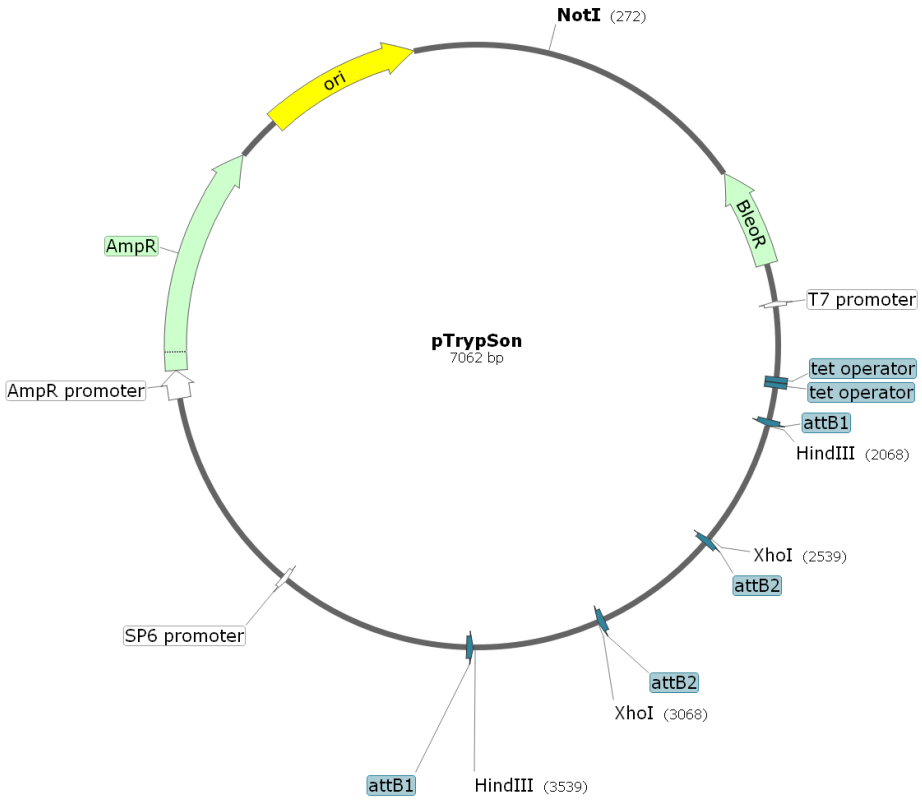

Fig.8. Map of pTrypSon vector (McAllaster et al., 2016). Xhol and HindII cleavage sites allow the insertion of inverted sequences between attB2 to generate hairpin loop RNAi. The Tet operator allows the controlled initiation of transcription in the presence of tetracycline via the T7 promoter and a NotI cleavage site to allow linearization near the flanks of homology. The ampicillin resistance marker allows selection in *E. coli*.

4.1.2.Plasmid Extraction

E. coli containing the pTrypSon vector was harvested to extract plasmid using the silica-binding/spin-column method of extraction in the GenElute Plasmid Miniprep Kit (Sigma-Aldrich). The bacterial culture was spun at 1300x g for 10 minutes at 10 °C with all supernatant removed, leaving the cell pellet. All subsequent centrifugations are done at 12000x g at room temperature. Bacteria were subsequently resuspended in 200 µl Resuspension Solution containing RNase A Solution and moved

into 1.5 ml Eppendorf tubes prior to vortexing. 200 µl of lysis solution was added and tubes were inverted 5 times to mix and left for 5 minutes to incubate, allowing membrane rupture. 350 µl of Neutralization/Binding Solution is added and tubes inverted 5 times to stop lysis procedure. Cell debris containing proteins, lipids and chromosomal DNA are pelleted by centrifugation for 10 minutes. Binding columns are prepared inside collection tubes with 500 µl Column Preparation Solution applied inside the column and spun for 2 minutes. Eluate is disregard from collection tube and the plasmid containing lysate is transferred into the binding column to be spun for 1 minute. Flow through is disregarded from collection tube and 750 µl Wash Solution is added into the column and spun once more for 1 minute. Flow through is disregarded and the Binding column placed inside a sterile 1.5 ml Eppendorf tube. One hundred µl of MiliQ H_2O is added and spun for 1 minute to elute plasmid DNA. The final plasmid concentration was measured using the NanoDrop 3300 (Thermo-Fisher) and stored in 4 °C.

4.1.3.PCR-Primers for RNAi and Gene Amplification

Based on IP results 9 to 11 proteins, including TbSam50, where shown to pulldown with TbMic10. Of these proteins, 8 where chosen for further analysis based on gene silencing of each individual protein via lhRNAi. The 7 potential MICOS candidates plus Sam50 were identified using mass spectrometry data (Table 1) and their corresponding DNA sequences found on the kinetoplastid genomic database: TriTrypDB.org.

Table.1. List of proteins identified in TbMic10-1/2 IPs. Proteins will be named based on established MICOS nomenclature (Pfanner et al., 2014).

Protein (Gene ID)	**MICOS nomenclature**
Tb927.9.10160	TbMic60
Tb927.11.6470	TbMic16
Tb297.5.690	TbMic17
Tb297.4.630	TbMic34
Tb297.2.2940	TbMic32
Tb297.10.11900	TbMic20
Tb297.5.580	TbMic40
Tb297.3.4380	Sam50

Oligonucleotide primers were designed in order to incorporate partial sequences of our gene of interest into the pTrypSon region between the two ‘Gateway’ sites. The Phusion High-Fidelity DNA Polymerase kit (NEB) was used to mediate the amplification of polymerase chain reaction (PCR) products. 33 µl MiliQ H_2O was combined with 200 µM dNTP, 3% DMSO, 0.2 µl Phusion DNA polymerase (2000 U ml^{-1}), 100-200 ng genomic *T. brucei* DNA, 1,25 µM reverse primer, 1,25 µM forward primer and 10 µl of 5X Phusion HF buffer to yield ~50 µl PCR solution. The negative control contained PCR mix without genomic *T. brucei* DNA. The PCR ran a total of 30 cycles using the following parameters (Table 2), based on primer melting temperature.

Table.2. Polymerase Chain Reaction parameters. Cycle from extension to denaturation was done 30x.

	Temperature in C°	Time in s
Initialization	98	300
Denaturation	98	15
Annealing	58	30
Extension	72	30
Final elongation	72	600
Final hold	14	Indefinite

4.1.4. PCR Cleanup

PCR products were purified using GenElute PCR Clean-Up Kit (Sigma-Aldrich) according to the manufacture's specifications. All centrifugations are done at 12000x g and room temperature. Binding columns are prepared inside collection tubes with 500 µl Column Preparation Solution applied inside the column and spun for 2 minutes. Eluate is disregard from the collection tube and 5 volumes of Binding Solution to 1 volume PCR product is added and spun for 1 minute. Flow through is disregard and 500 µl Washing Solution is applied to the column and centrifuged as above. The Binding column is placed inside a sterile 1.5 ml Eppendorf tube. 100 µl of MiliQ H_2O is added and spun for 1 minute to elute purified PCR product. Final concentration was measured using the NanoDrop 3300 (Thermo-Fisher) and stored at 4 °C.

4.1.5. Digestion

Our unmodified pTrypSon contains the unwanted TbCentrin sequence between the AttB1 and AttB2 region, the vector contains 2 cleavage sites with the ability to excise this sequence using restriction enzymes HindIII and XhoI, allowing for the insertion of our PCR product (Figure 7). 400-600 ng μl^{-1} pTrypSon plasmid was incubated with 1 µl High Fidelity-HindIII (20 000 U ml^{-1}) (NEB) and 4 µl complimentary Cutsmart buffer (NEB) in 15 µl MiliQ H_2O at 37 °C for 1 hour[1] to yield the vector 'backbone' and AttB1 region. Similarly 400-600 ng μl^{-1} pTrypSon plasmid was incubated with 2 µl XhoI (20 000 U ml^{-1}) (NEB) and 4 µl complimentary Cutsmart buffer (NEB) in 15 µl MiliQ H_2O at 37 °C for 1 hour to yield the 'stuffer' and AttB2 region (Figure 7).

4.1.6. Verification and Gel Purification of Vector Components and PCR Products

Both PCR products and vector components were verified prior to cloning using agarose gel electrophoresis. The gel was cast using 1 g of agarose in 100 ml of 1X Tris-acetate-EDTA (TAE) buffer solution (40 mM Tris, 20 mM acetic acid and 1 mM EDTA). The mixture was brought to a boil and cooled before addition of 50 µg ethidium bromide (ThermoFisher) and cast on the apparatus. The gel was then submerged in a solution of 50 ml 1X TAE and 450 ml H_2O before addition of our DNA of interest containing 8 µl 6X glycerol DNA loading buffer (ThermoFisher) into the wells. The voltage was set to 90 V and left to run until the bromophenol blue dye migrated towards the end of the gel. DNA was visualized using Image Lab software (Bio-Rad).

[1] No longer than 1 hour to prevent Star activity with HF-HindIII

PCR products were examined to have to the correct molecular weight while vector components were excised from the gel to purify. DNA was visualized under UV-light and excised from the gel. The vector components were purified using the GenElute Gel Extract Kit (Sigma-Aldrich) according to the manufacture's specifications. The excised gel band was weighted and solubilized using 3 volumes (3:1 volume to weight) of Gel Solubilization Solution inside a 1.5 ml Eppendorf tube for 10-15 minutes until completely dissolved at 55 °C. All subsequence steps are identical to the PCR Cleanup procedure in 4.1.4.

4.1.7. Gibson Assembly

Both vector fragments and PCR products were purified prior to assembly. The vector backbone was treated with alkaline phosphatase (20 U μl^{-1}) (Promega) for 1 hour at 37 °C prior to assembly to prevent backbone self-ligation. All three fragments were combined using homemade Gibson Assembly Master Mix. The homemade Master Mix was prepared by combining 320 µl 5x isothermal reaction buffer (3 ml 1M Tris-HCl pH 7.5, 150 µl 2M $MgCl_2$, 60 µl 100 mM dGTP, 60 µl 100 mM dATP, 60 µl 100 mM dTTP, 60 µl 100 mM dCTP, 300 µl 1 M DTT, 1.5 g PEG-8000, 300 µl 100 mM NAD, and addition of ddH_2O to 6 mL), 0.64 µl T5 exonuclease (10 U μl^{-1}), 20 µl Phusion DNA polymerase (2U μl^{-1}), 160 µl Taq DNA ligase (40 U μl^{-1}) and addition of MiliQ H_2O to 1200 µl. The solution was aliquoted at 20 µl and stored at -20 °C for long term storage. The fragment to vector ratio varied based on DNA concentration. Typically a 3:2:4 (backbone: stuffer: PCR product) concentration ratio was used during the procedure, as I determined this yields better results compared to the previously published ratio of 1:1:5 (McAllaster et al., 2016). The mixture was subsequently incubated in a 50 °C heat bath for 60-90 minutes.

4.1.8. Transformation into Competent Cells

Newly assembled plasmids were introduced into the XL-1 Blue Competent *E. coli* cell line (Agilent Technologies) via conventional heat-shock treatment. *E. coli* cells were placed on ice to defrost for 15 minutes before mixing ca. 10 µl plasmid and 100 µl cells by pipetting gently up and down. The solution was then set on ice for 30 minutes before heat-shocking at 42 °C for 30-60 seconds. The solution was then placed on ice once more for 5 minutes prior to addition of 250 µl Super Optimal Broth containing 20 mM glucose (SOC) (Thermo Fisher) medium and incubated at 37 °C on 200 rpm for one hour.

Cultures were then spun at 1100x g for 2 minutes and excess SOC was removed before applying bacterial suspension onto ampicillin containing lysogeny broth (LB) agar dishes by spreading with an L-shaped cell spreader and incubated overnight at 37 °C.

4.1.9. Verification of Plasmid

Correct vector assembly was initially verified using colony PCR to confirm the presences and correct orientation of all four fragments. Six to eight colonies were chosen at random from agar plates. The colony of choice was removed using a pipette tip and submerged in 2 PCR tubes containing 7.5 µl dH_2O each before tip was introduced on another ampicillin containing LB agar dish and marked. PCR tubes containing cells were lysis at 95 °C using a heat bath for 4 minutes before addition of 12.5 µl

commercial PPP Master Mix (150 mM Tris-HCl, pH 8.8, 40 mM $(NH_4)_2SO_4$, 0.02% Tween 20, 5 mM MgCl2, 400 µM dATP, 400 µM dCTP, 400 µM dGTP, 400 µM dTTP, 100U ml^{-1} Taq DNA polymerase and dye) (Top-Bio), 1.25 µM forward primer and 1.25 µM reverse primer. The PCR reaction ran using the previous program (Table 2). The PCR negative control was done by addition of unmodified pTrypSon plasmid in replacement of colony DNA.

In order to ensure that both our inserts are present within the vector and in the correct orientation, the PCR ran using two samples of the same colony. One reaction contained the forward RNAi primer and forward pTrypSon primer while the second contained the forward RNAi primer and reverse pTrypSon primer (Figure 9).

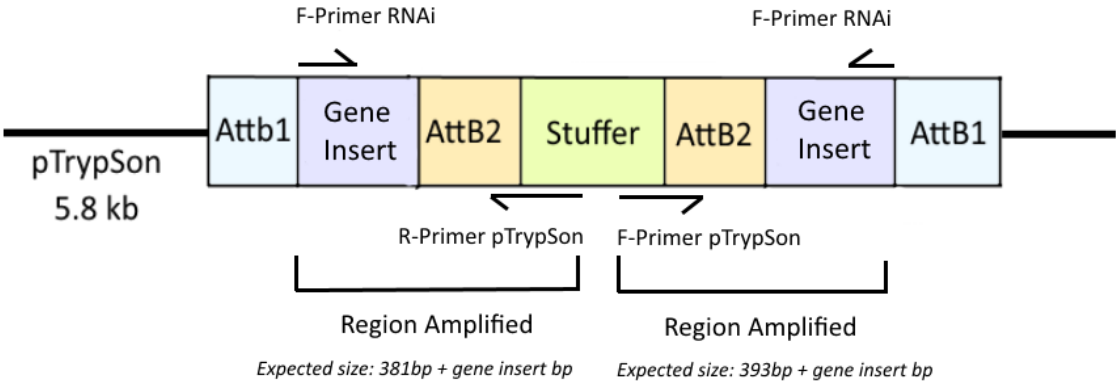

Fig.9. Schematic depicting how PCR can verify if both or only one insert is present inside the vector. Since pTrypSon primers do not anneal dead-center of the 'stuffer' both bands will be of different molecular weight, further verifying the presence of both inserts.

The molecular weight of the bands was examined by agarose gel electrophoresis using the same procedure as in section 4.1.6. The exact molecular weights of the bands were calculated using the following formula:

Band containing forward pTrypSon primer: 393bp + number of bp in gene insert = weight of band

Band containing reverse pTrypSon primer: 381bp + number of bp in gene insert = weight of band

Sanger sequencing of our finalized vector was done to inspect if any polymorphic positions were present after generation of sufficient plasmid (see 4.1.10). Errors within the sequence, *e.g.* polymorphic positions, could yield less efficient RNAi, due to decreased recognition of target mRNA and to a lesser extent hairpin loop stability. Sequencing was provided by Eurofins Genomics.

4.1.10. Transfer to Liquid Media and Plasmid Extraction

The colony of choice, based on colony PCR results, was grown in 15 ml test tubes containing LB media and inoculated with 2.5 µg ml^{-1} ampicillin. Cultures were incubated for 24 hours shaking at 200 rpm at 37 °C. Final plasmid constructs were extracted from *E. coli* cultures using the GenElute Plasmid Miniprep Kit (Sigma-Aldrich) following the same procedure as mentioned in section 4.1.2

4.2. Transfection of Trypanosoma brucei

4.2.1. Electroporation of Procyclic Trypanosoma brucei

Constructs were linearized prior to transfections by addition of 3 µl high fidelity Not-I (10 000 U ml^{-1}) (NEB) restriction enzyme in a 10µl solution of Cutsmart buffer (NEB) for 10 µg DNA in 87 µl dH2O and left overnight at 37 °C. DNA precipitation was done by addition of 250 µl 96% ethanol and 10 µl 3 M sodium acetate (pH 5.2) and left in -20 °C for 1 hour. DNA was subsequently spun at 4 °C for 15 minutes at 12500x g with all supernatant being removed and left to dry.

The *T. brucei* 927 strain SmOxP cell line (Poon et al., 2012) served as the parental cell line, already modified to bear TbMic10-1 V5-tagged and each individual subunit HA-tagged (Kaurov et al., submitted). Each subunit was *in situ* C-terminally tagged, save the N-terminally tagged Sam50. Ten ml SmOxP cell lines were harvested at mid-log phase 1-2 $\times 10^7$ cells/ml by centrifugation at 4 °C for 10 minutes at 1300x g. All the supernatant was removed via pipetting. Ten ml Cytomix buffer (25 mM HEPES pH 7.6, 120 mM KCl, 0.15 mM $CaCl_2$) was used to wash cell pellet by resuspension, cells were then spun once more at 4 °C for 10 minutes at 700 g with supernatant removed.

Linearized construct of choice was resuspended in 100 µl Amaxa Human T-cell Nucleoefector solution (81.8 µl Human-T cell and 18.2 µl Supplement 1) (Lonza) and used to resuspend SmOxP cell pellet prior to being loaded on cuvettes. Cells were electroporated once under the Amaxa X-001 program (Lonza) then resuspended in 10ml SDM79 medium containing 2.5 µg ml^{-1} hygromycin, 2.5 µg ml^{-1} puromycin and 2.5 µg ml^{-1} geneticin for 18 hours at 5% CO_2 and 25 °C conditions.

4.2.2. Cell Culturing

Tranformants were selected via addition of 0.5 µg ml^{-1} phleomycin to 10 ml cultures. These cultures were further separating into 24 (6 x 4) well plates for limiting dilution to yield pseudoclones (Figure 10). One and a half ml of culture was transferred onto the first row; with the following second and third row containing 1ml fresh SDM79[2] medium and the fourth row containing 0.5 ml fresh SDM79. Five hundred µl of cell containing culture from the first row was transferred into the second row and the process was repeated with the following rows. The 24 well plate cultures were kept incubated at 27 °C for 10-13 days while selection continued with cultures being constantly diluted with fresh antibiotic cocktail medium until the negative control cells expired, as seen under light microscopy.

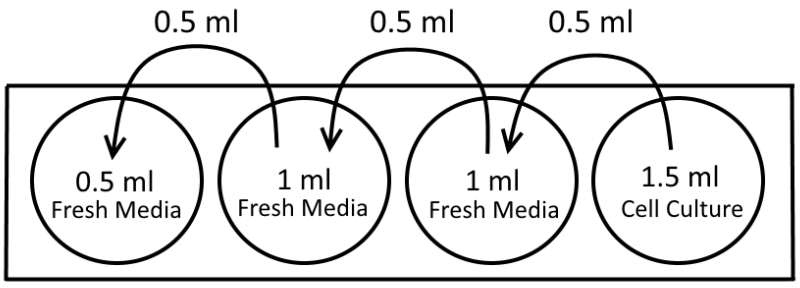

Fig.10. Schematic for limiting dilution.

[2] All subsequent SDM79/80 media contain an antibiotic cocktail of 2.5µg ml^{-1} hygromycin, 2.5µg ml^{-1} puromycin, 2.5µg ml^{-1} geneticin and 5µg ml^{-1} phleomycin for all cell lines except Sam50, where geneticin is substituted for 5µg ml^{-1} blasticidin

4.2.3. Selection of Clones via Western Blotting

Cell clones that survived antibiotic treatments were then further selected based on RNAi efficiency. Individual cell line clones were transferred into larger flasks in duplicates for RNAi induced and non-induced cultivation. RNAi activated cultures were induced with 1 µg ml^{-1} doxycycline on hour 0 and hour 48 during the incubation 96 hour period prior to harvesting. Induced and non-induced cells were harvested at the same time to minimize differences in sample collection. The detailed methodology of sample preparation for LDS-PAGE, LDS-PAGE and Transferring procedures are described in sections 4.4.1.- 4.4.3.

After overnight blocking in milk, the membrane was cut near the 55 kDa section in order to separate antibody incubation of HSP70 (loading control, 70 kDa) and HA-tagged TbMICOS proteins (12-52 kDa range). The primary antibody (Table 3) was combined in 1x PBS-T containing 4% (w/v) powered milk and incubated on membranes for 2 hours at room temperature in constant rotation. Membranes were then washed three times with 1x PBS containing 0.5% (v/v) Tween 20 in 10 minute intervals. The secondary antibody was combined in 1x PBS containing 4% (w/v) powered milk and 0.5% (v/v) Tween 20 and incubated on membranes for 1 hour at room temperature in constant rotation. Membranes were washed using the same procedure mentioned above. The Clarity Max Western ECL Blotting Kit (Bio-rad) protocol containing Clarity Max Western Peroxide Reagent and Clarity Max Western Luminol/Enhancer Reagent (1:1 mixture, 400 µl total) was spread out on the membrane to allow chemiluminescent detection of the proteins using Image Lab software (Bio-Rad), according to manufacturer's specifications.

4.3. Measurement of Cell Fitness

4.3.1. Growth Measurements on Glucose Rich and Glucose Poor Media

Induced and non-induced cell cultures were monitored for 6 days of growth analysis at 27 °C. Densities of cells were measured using the Beckman Coulter Z2 Particle Counter every 24 hours with cells begin diluted back to 2×10^6 cells/ml and induced with 1µg ml^{-1} doxycycline daily. All measurements were done in triplicate with three cultures in 1 µg ml^{-1} doxycycline media solution and three cultures 1 µg ml^{-1} pure ethanol media solution as a control. Mean values were calculated and graphed. Growth was examined both in 6 mM glucose-rich medium and no glucose-added medium, SDM79 and SDM80 respectively.

4.4. Protein Analysis

4.4.1. Cell Culturing and Sample Preparation for LDS-PAGE

Cell cultures were induced with 1µg ml^{-1} doxycycline once every 48 hours for 2, 4, and 6 day post induction growth analysis. Cell cultures were grown at 27 °C on a shaker to facilitate gas exchange. Day 0, 2, 4, and 6 post inductions cells were harvested at the same time to minimize differences in sample collection. 1×10^8 cells were collected and transferred to 15 ml tubes and spun at 12 °C for 10 minutes at 1300x g. The majority of supernatant was removed and spun once more with the same parameters for 3 minutes to insure minimal loss of cells. All remaining supernatant was then removed via pipettes. One ml 1x phosphate-buffered saline (PBS) (137 mmol NaCl, 2.7 mmol 2.7 KCl, 10 mM Na_2HPO_4, 1.8 mmol KH_2PO_4) solution was added to each cell pellet and washed in 1.5 ml Eppendorf

tubes. Tubes subsequently spun again at 12 °C for 10 minutes at 1300x g with all remaining PBS removed through careful pipetting. The washing procedure was repeated twice with fresh 1x PBS. Cell pellets were then resuspended in 75 µl 1x PBS and 25 µl 4x lithium dodecyl sulfate (LDS) loading buffer (ThermoScientific) with the final concentration being 1×10^8 cells in 100 µl samples. Samples were then placed on a heating block at 85 °C for 5 minutes before being run on PAGE-gels, according to manufacturer's specifications.

4.4.2. LDS-PAGE

Samples were sonicated at 40% for 5 seconds once thawed. 5% 2-(N-morpholino)ethanesulfonic acid (MES) running buffer was prepared from 20x MES stock solution (ThermoScientific) and 475 ml dH_2O. Bolt TM 4-12% Bis-Tris Plus gels (ThermoScientific) were treated prior to sample loading by gentle pressure to clean the wells with MES buffer via syringe. Samples were loaded and then ran at 180V until bromophenol blue dye migrated near the bottom of the gel.

4.4.3. Western Blotting

Western blotting of LDS-PAGE separated proteins on methanol pretreated nitrocellulose membranes, using cooled transfer buffer (25 mM Tris base, 190 mM glycine and 20% methanol). Ice packs were added to the apparatus to prevent overheating while running at 120V for ca. 2 hours. Blocking of the membranes consisted of an overnight treatment at 4 °C using 1x PBS-T containing 4% (w/v) powered milk.

Table.3. Antibodies used to detect expression levels

Primary Antibody (Source)	Secondary Antibody	Dilution Primary	Dilution Secondary
Anti-HA (ThermoScientific)	Anti-Mouse	1:2000	1:1000
Anti-V5 (ThermoScientific)	Anti-Mouse	1:2000	1:1000
Anti-VDAC (Pusnik et al., 2009)	Anti-Rabbit	1:500	1:1000
Anti-TbERV1 (Basu et al., 2013)	Anti-Rabbit	1:1000	1:1000
Anti-ATPase (Speijer et al., 1997)	Anti-Rabbit	1:500	1:1000
Anti-HSP70 (Kenneth Stuart, Center for Infectious Disease Research, Seattle, USA)	Anti-Mouse	1:1000	1:1000

Similar to the methodology stated in section 4.2.3. membranes were probed with primary antibodies targeting different mitochondria proteins (Table 3) with chemiluminescent detection done using Image Lab software (Bio-Rad), according to manufacturer's specifications.

4.5. Sample Preparation for Transmission Electron Microscopy

4.5.1. Cell Culturing and Sample Collection

Cristae morphology was examined by transmission electron microscopy (TEM). Cell cultures were induced with 1µg ml^{-1} doxycycline once every 48 hours for 2-3 days and harvested for morphology analysis. Cell cultures were grown at 27 °C on a shaker to facilitate gas exchange. Cultures were grown to 20 ml with a dense concentration of 1-2 × 10^7 cells/ml. All RNAi induced cell lines, along with the parental cell line were centrifuged at 1300x g for 10 minutes at 12 °C prior to being transferred to the Laboratory of Electron Microscopy for high-pressure freezing and TEM imagining.

5. Results

5.1. Construct Verifications and RNAi Assessment

The generation of constructs for RNAi was done using the established pTrypSon vector (Figure 8). The vector was digest to isolate the backbone using HindIII and Xhol. Our gene of interest was amplified using PCR and subsequently verified using gel electrophoresis.

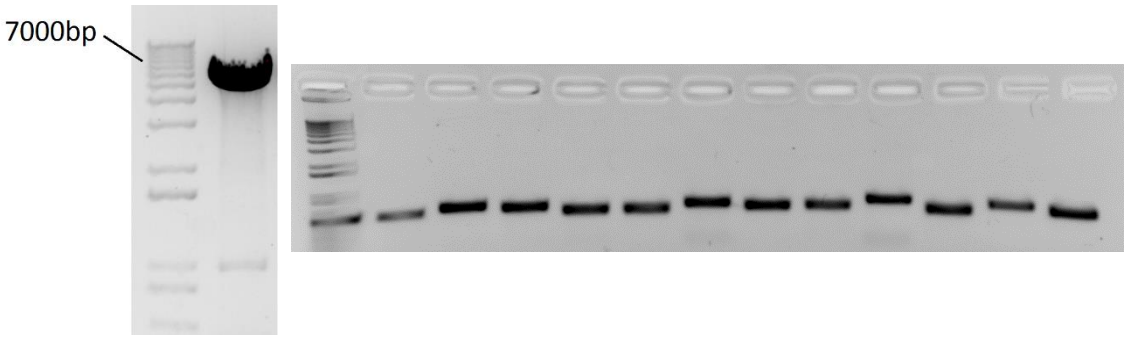

Fig.11. Gel electrophoresis verifying both extraction of pTrypSon backbone (left) and RNAi inserts for cloning into the backbone vector based on PCR (right). All bands were verified to contain the correct molecular weight and no contamination prior to Gibson cloning.

Prior to transfection into *T. brucei*, constructs were verified to contain both desired inserts of different molecular weight (Figure 9). This was mediated through colony PCR. Colonies containing both bands with similar intensity were chosen for transfection (Figure 12).

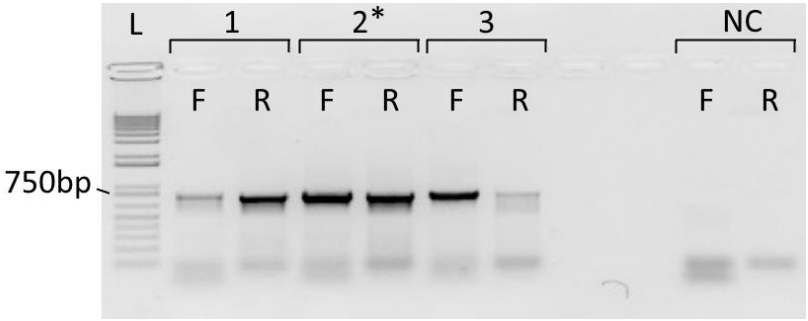

Fig.12. Verification based on colony PCR of *E. coli* containing constructs for Mic32 RNAi. Colony containing asterisk (No. 2) was chosen based on similar band intensity for both reversed and forward primers (Explanation of band size and intensity on Figure 9). This verification was done on all constructs prior to transfection in *T. brucei*. L stands for 'DNA ladder', NC for negative control.

After transfection and selection in *T. brucei*, RNAi efficiency was assayed through immunoblotting. Clones were split into two cultures, with one serving as the control (non-tetracycline induced) and one to examine RNAi efficiency (tetracycline induced). The clone containing the lowest expression of the HA-tagged protein after 4 days post induction was chosen to for all subsequent experimentations (Figure 13).

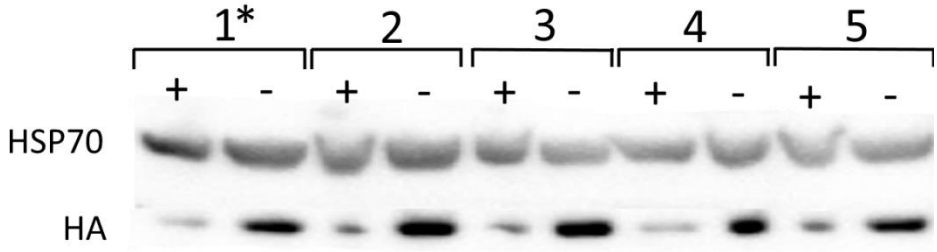

Fig.13. RNAi efficiency for TbMic20 knockdown cell lines was evaluated based on immunoblot analysis. Protein of interest was HA-tagged with clones split into RNAi induced (+) and non-RNAi induced (-) to measure efficiency of controlled depletion. Tetracycline was induced for 4 days before harvesting. Clone containing asterisk (No. 1) was chosen based on near total depletion of HA signal. This verification was done on all constructs prior subsequent experimentations. HSP70 serves as a loading control.

5.2. Individual TbMICOS Subunits are Vital for Cellular Growth

To address the functional role of TbMICOS subunits and TbSam50 in regards to cellular growth, *T. brucei* strains allowing the controlled depletion of single MICOS subunit were generated. Using this approach, growth of cell lines was examined in both glucose-rich and glucose-poor medium in triplicate. All cell lines, with the exception of TbMic16, showed growth arrest on day 2-3 post RNAi activation under both conditions compared to the negative control. Growth arrest persists throughout RNAi inductions. Surprising is the growth inhibition in glucose-rich medium (Figure 14), as similar studies on yeast growth on fermentable medium did not result in growth arrests when MICOS subunits were depleted (Friedman et al., 2015). Since growth inhibition appears under both conditions, it can be concluded that TbMICOS subunits are crucial for procyclic *T. brucei* fitness, regardless whether OXPHOS is utilized (Figure 14; Figure 15) (Coustou et al., 2008). TbSam50 depletion similarly shows compromised growth under both conditions within the same time frame as the other TbMICOS subunits. The apparent similarity of impaired cell fitness between TbMICOS subunits suggests that TbMICOS contains components that are vital to maintain cellular growth, despite the bioenergetic state of the mitochondria.

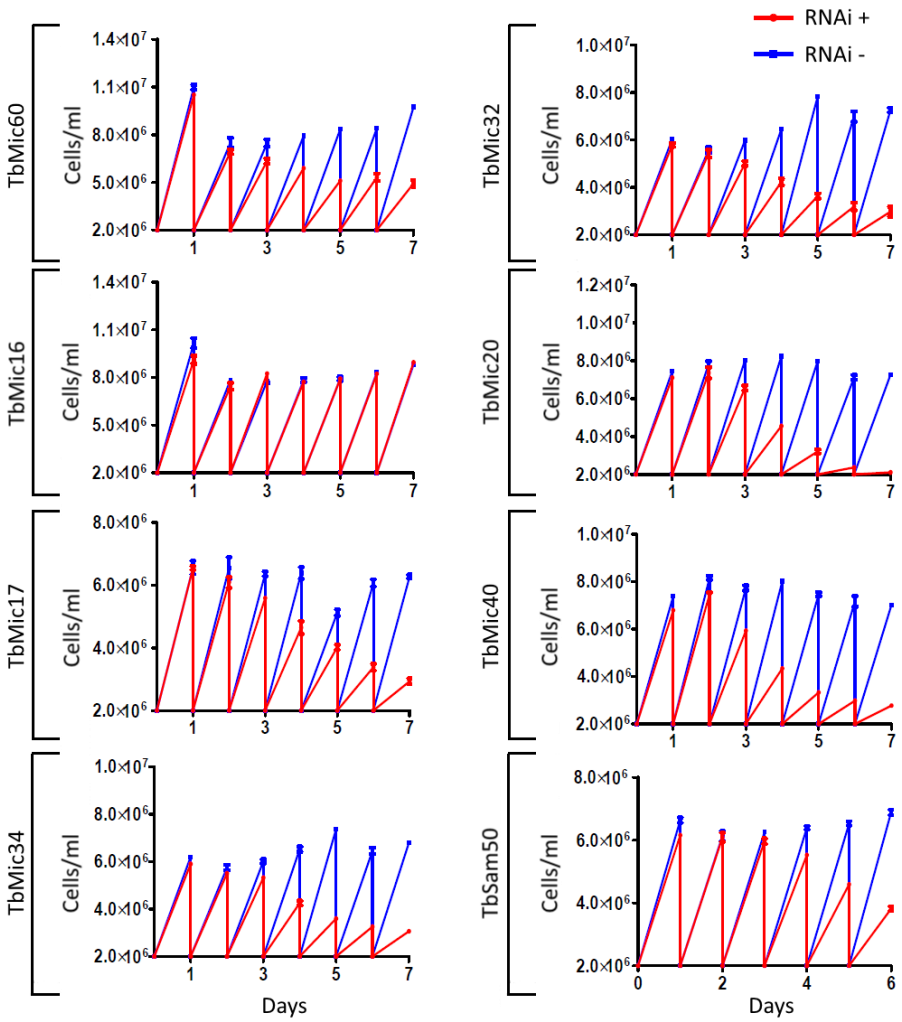

Fig.14. Measurements of TbMICOS RNAi growth in glucose-rich medium. Growth analysis was done in triplicates with standard deviation shown with error bars (n=3). Y-axis, cell density; X-axis, days post RNAi induction. Cell lines indicated next to left brackets.

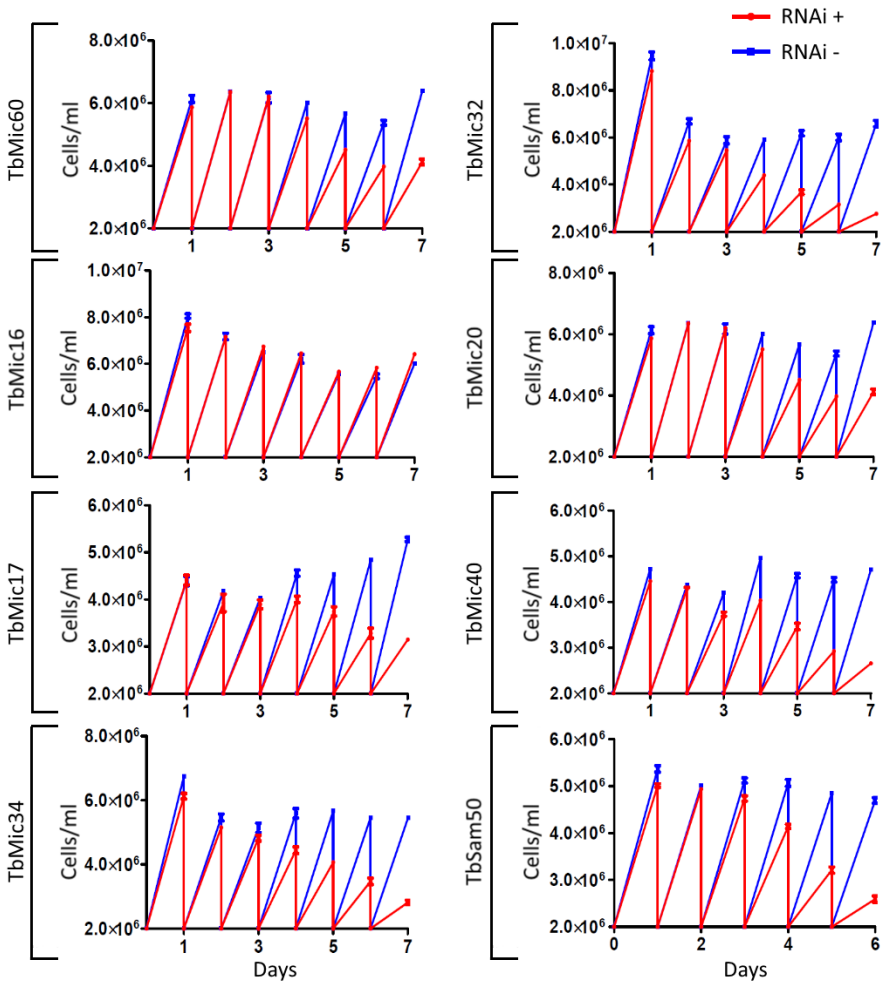

Fig.15. Measurements of TbMICOS RNAi growth in glucose-poor medium, as depicted in figure 14.

5.3. Knockdown of Individual TbMICOS Subunits Result in Depletion of TbMIC10-1

After establishing that TbMICOS subunits are essential to maintaining *T. brucei* fitness, regardless of the bioenergetic condition of the mitochondrion, we examined whether depletion of these subunits would result in altered levels of TbMic10-1. In order to examine steady-state levels, *T. brucei* strains containing both the V5-tagged TbMic10-1 and the HA-tagged subunit allowed us to simultaneously track expression levels of both TbMic10-1 and the subunit during RNAi inductions. Over a 6 day RNAi induction time course, all cell lines, including TbSam50, showed altered levels of TbMic10-1 expression (Figure 16). Of all the subunits, only TbMic17 did not show a downregulation of TbMic10-1. Interestingly, TbMic32, TbMic20 and TbMic40 knockdowns only resulted in partial TbMic10-1 depletion, while TbMic60, TbMic16 and TbMic34 knockdowns yield near complete loss of TbMic10-1 levels. Protein expression levels were standardized using HSP70 as a loading control. Since downregulation of TbMic10-1 appears to be consistent throughout the silencing of the majority of the targeted proteins, it can be stated that these subunits interact with the complex.

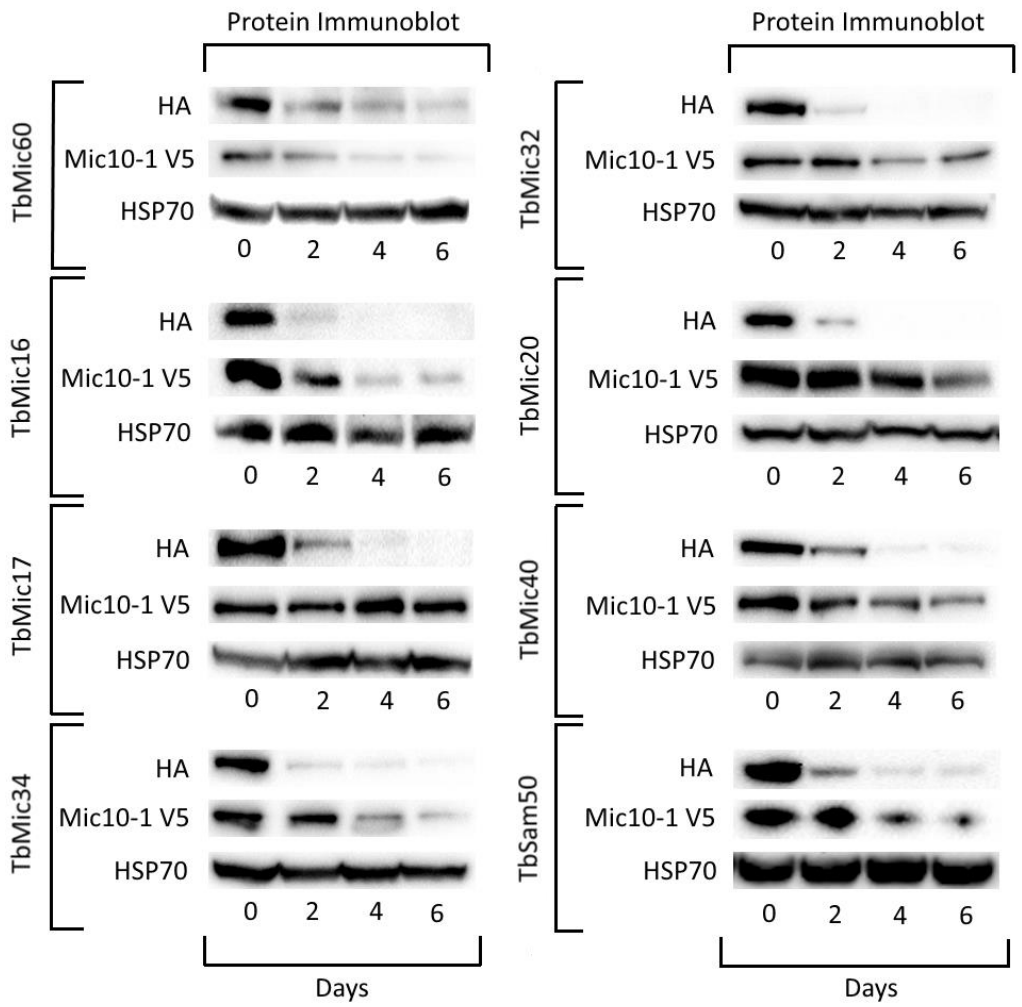

Fig.16. Immunoblot analysis indicating successful knockdown of gene of interest (HA-tagged) and resulting steadystate levels of TbMic10-1 (V5-tagged). HSP70 serves as a loading control. Days post RNAi induction shown on bottom. Cell lines indicated to the left of brackets.

5.4. Knockdown of Individual TbMICOS Subunits Result in Altered Cristae

The role of these subunits was further investigated by examining knockdown effects on cristae morphology. Ultrathin cryosections of all RNAi cell lines were produced at time points immediately prior to growth arrest. TEM preparation and imaging was performed at the Laboratory of Electron Microscopy, Biology Centre CAS, České Budějovice, Czech Republic.

Both TbMic60 and TbMic20 exhibit elongated cristae with a circular morphology, as compared to the parental control (Figure 17). TbMic32 and TbMic34 result in a lesser elongated cristae phenotype compared to TbMic60 and TbMic20 data. Interestingly, TbMic40 bares distinctive mitochondrial blebbing accompanied with rounded cristae (Figure 17). TbSam50 appears to not yield elongated cristae when knockdown. The majority of RNAi knockdown cell lines show altered cristae morphology, some more severe than others, suggesting that most TbMICOS components are needed to maintain proper cristae formation, with the exception of TbSam50, TbMic16 and TbMic17.

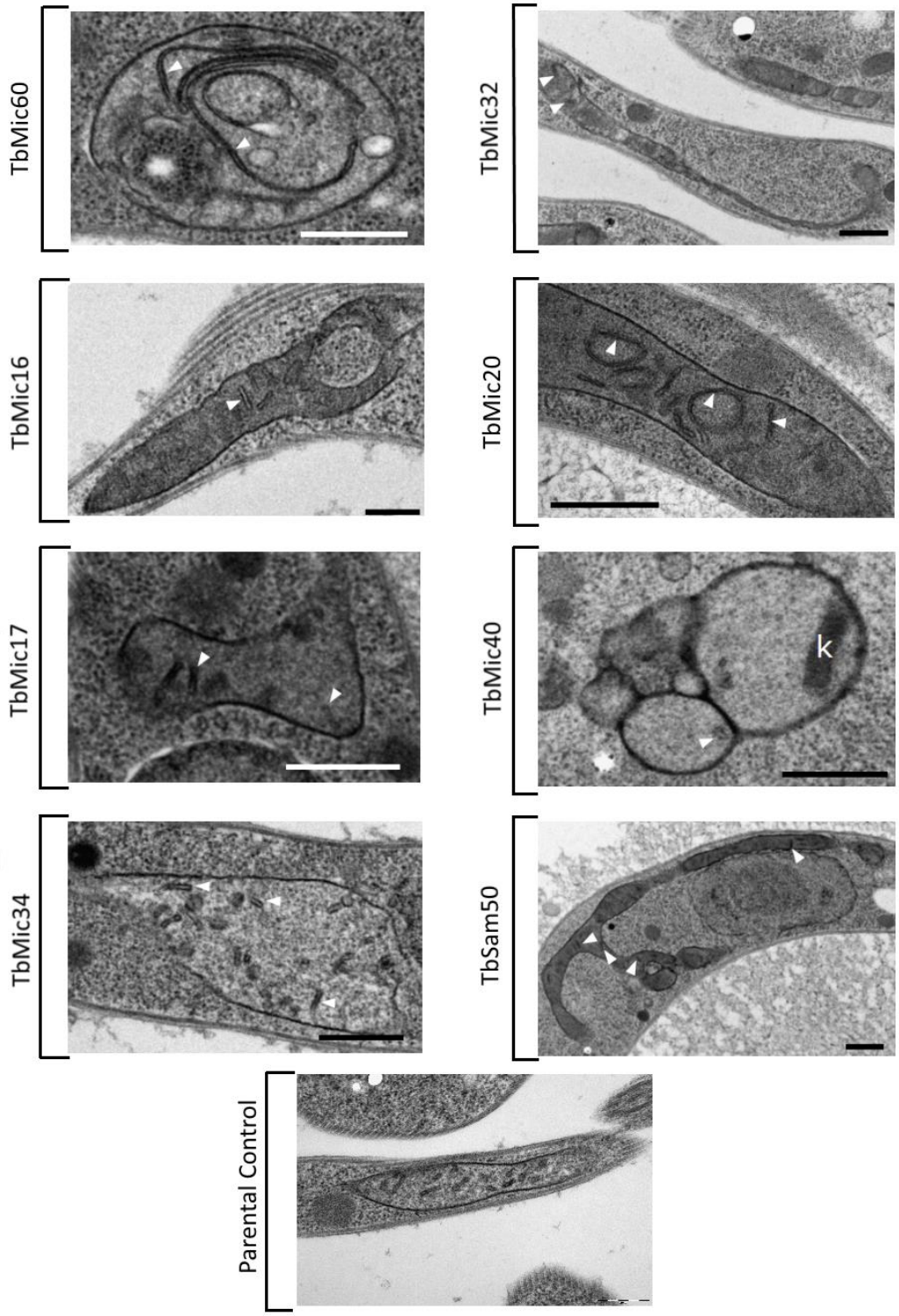

Fig.17. TEM imaging of individual TbMICOS subunit RNAi knockdowns. Imagining was done at day 2 post RNAi induction for cell lines TbSam50 and TbMic40, all others at day 3. Non-RNAi induced SmOxp cell line served as the parental control. Arrowheads point to cristae. Bars, 500 nm. Images by Hashimi H. & Kaurov I.

5.5. TbMICOS Silencing Results in Depleted Levels of TbERV1

Given that MICOS is known to interact with various proteins throughout the mitochondria, subsequent analysis was taken to verify if these proteins influenced other mitochondrial proteins. In order to investigate possible effects of TbMICOS knockdowns on different mitochondrial proteins, all RNAi cell lines were probed for altered levels of F_OF_1-ATP synthase β subunit, voltage-dependent anion channel (VDAC), and TbErv1 (Figure 18). The F_OF_1-ATP synthase β subunit was not affected by RNAi silencing in any of the cell lines. This result is somewhat surprising, as ATP synthase also mediates membrane curvature in cristae via its V-shape dimers (Davies & Kuhlbrandt 2018; Anselmi et al., 2018).

VDAC was only altered upon TbSam50 depletion, which complies with the contribution of Sam50 in protein import into the MOM (Hohr et al., 2018). However this was not the case for any of the TbMICOS subunits. Intriguing however, is the downregulation of TbErv1 in TbMic16, TbMic32 and TbMic20 knockdowns on the fourth day, similar to the time range of TbMic10-1 depletions in TbMic16 and TbMic32 (Figure 18; Figure 16). Nevertheless, only TbMic20 does not show such a drastic decrease in TbMic10-1 levels in comparison to TbMic16 and TbMic32, garnering interest for this particular subunit.

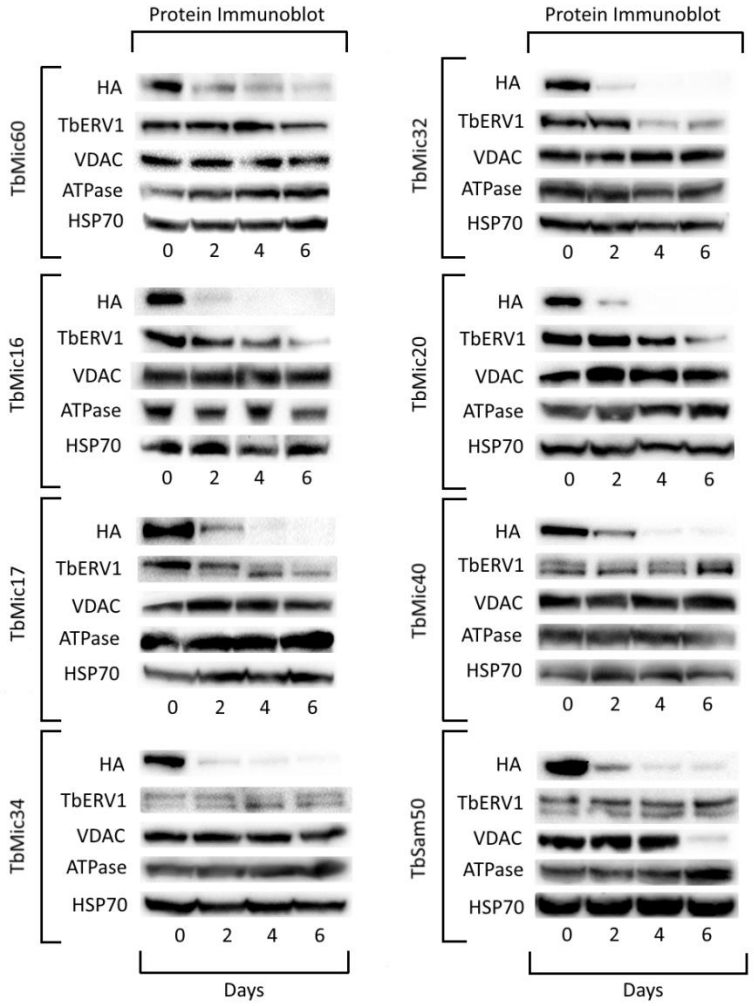

Fig.18. Immunoblot analysis depicting expression levels of different mitochondrial proteins in RNAi cell lines. HSP70 serves as the loading control. X-axis, days post RNAi induction. Cell lines indicated on left brackets.

As it appears, the majority of all TbMICOS subunits, including TbSam50, play a significant role in the stabilization of TbMic10-1 (Figure 16). However, knockdowns of TbMic16, TbMic17 and TbMic20 yield an unexpecting drop in TbErv1 (Figure 18). The depletion of this IMS protein suggests that TbMICOS may interact with the MIA pathway. TbErv1 plays a central role in this pathway, as seen by reduced IMS protein levels when knockdown in procyclic *T. brucei* (Peikert et al., 2017). Erv1 relays with Mia40 to facilitate the introduction of disulfide bonds in unfolded IMS proteins in opisthokonts. This is achieved by the ability of Erv1 to reoxidize the CPC reaction center in Mia40 (Figure 7; Figure 19). Currently, a functional Mia40 homolog has yet to be identified in *T. brucei* (Haindrich et al., 2017).

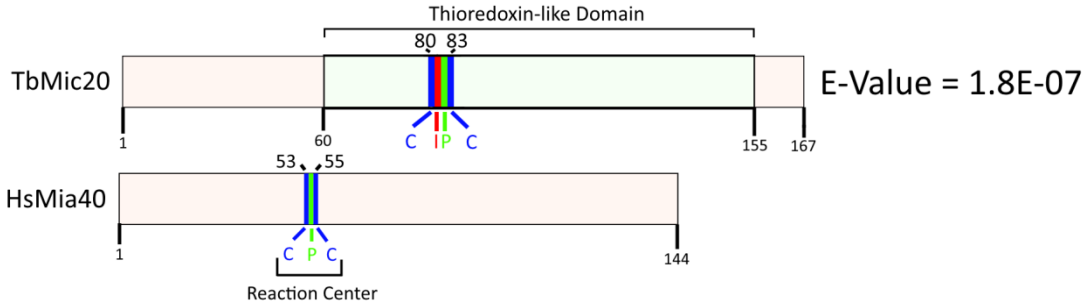

Fig.19. Schematic comparison of TbMic20 (top) and HsMia40 in *H. Sapien* (bottom). The predicted thioredoxin domain (in light green) in TbMic20 contains a CIPC motif that may function in a similar matter as the CPC reaction center in HsMia40. E-value predicted by Pfam 31.0v

TbMic20 gained further interest, as the sequence contains a CIPC motif, similar to the CPC reaction center of Mia40 in humans (Figure 19). This predicted thioredoxin-like protein could hold the potential to relay with TbErv1 to mediate the introduction of precursor proteins into the IMS. The presence of this thioredoxin-like domain along with reduced levels of TbErv1 in TbMic20 serves as a good indicator that TbMICOS may indeed be involved in the MIA pathway.

6. Discussion

This work is a portion of a much larger investigation into the revolutionary study of MICOS outside of opisthokont models. In this study, we investigate conserved properties, as well as potential novel features of MICOS. As an evolutionary conserved complex, MICOS may provide insight into the biogenesis of the mitochondria through functional analysis of preserved features throughout diverse eukaryotes. Belonging to the excavate supergroup, the diverged *T. brucei* allows us to study these novel features. There are 6 to 7 subunits that associate with MICOS in humans and yeast, while TbMICOS comprises 8 stably interacting proteins, including the conserved interaction partner Sam50. In yeast, Sam50 interacts with MICOS via the mitofilin domain in Mic60 (Bohnert et al., 2012; Korner et al., 2012), which is lacking in TbMic60 (Kaurov et al., submitted). However, gene silencing of TbSam50 results in depletion of TbMic10-1, indicating a stable interaction with TbMICOS. The interaction between TbSam50 and TbMICOS appears to take place without a mitofilin domain, hinting at a novel feature of MICOS.

TbMICOS also contains other candidates that lean towards the idea of novel complex components with non-redundant roles. Gene silencing of the majority of individual TbMICOS subunits result in

altered cristae morphology. While certain subunits show more extreme disturbances in cristae formation than others, TEM imaging depicts a similar trend among the majority of knockdowns: elongated cristae (Figure 17). Comparably, immunoblot analysis also suggests that most TbMICOS subunits interact strongly with TbMic10-1, with TbMic60, TbMic16 and TbMic34 knockdowns contributing to near complete downregulation of TbMic10-1 levels (Figure 16). Indeed, all 8 subunits presented appear to form a genuine complex in *T. brucei*.

Knockdowns of MICOS in yeast reveal redundant roles for certain subunits, proposed to be due in part of a functionality hierarchy (Ott et al., 2015). TbMic16 turns out to be the only subunit that does result in growth arrest after RNAi silencing, with all other subunits showing growth arrest within the same time frame of 2-3 days post RNAi induction (Figure 14; Figure 15). The lack of both altered cristae morphology and growth phenotype in TbMic16 indicates that the subunit is not vital for maintaining cell fitness, but nevertheless forms part of the TbMICOS complex due to downregulation of TbMic10-1 (Figure 17; Figure 16). This supports the idea of a MICOS hierarchy in *T. brucei*, as studies on opisthokont MICOS propose that depletion of peripheral subunits do not result in severe negative phenotypes, forming the basis of a MICOS hierarchy (Ott et al., 2015).

More interesting however, is the compromised growth in medium supplied with glucose (Figure 14), as OXPHOS is not utilized under such conditions for procyclic *T. brucei* (Coustou et al., 2008). This differs drastically from results of complete MICOS knockdowns in yeast, as yeast grown under fermentable conditions did not result in growth arrest (Friedman et al., 2015). This fitness impairment due to individual TbMICOS subunit ablations under glucose-rich medium demonstrates the importance of the complex in sustaining vitality in *T. brucei*.

All RNAi cell lines were investigated to verify any influences between subunit knockdowns and other mitochondrial proteins. The F_OF_1-ATP synthase β subunit was not downregulated or upregulated in any of the RNAi cell lines. Since ATPase dimers are present throughout cristae to mediate membrane curvature, an upregulation would have been expected due to elongated cristae as seen in TEM imaging (Figure 17: Figure 18) (Davies & Kuhlbrandt 2018). However this was not the case for any TbMICOS subunits. Moreover, studies on yeast Mic60 show that its depletion results in increased levels of F_OF_1-ATP synthase supercomplexes, while overexpression shows decrease levels of these supercomplexes (Rabl et al., 2009). Mic10 is also known to bind to the F_OF_1-ATP synthase in yeast, selectively associating with the dimeric forms and supporting the formation of oligomers (Rampelt et al., 2017b). In our study, TbMic60 depletion shows no apparent effects on the F_OF_1-ATP synthase β subunit levels, nor do any other TbMICOS subunits. However, it may be very well possible that certain TbMICOS subunits affect different subunits of ATPase in *T. brucei*. This is of interest due to the apparent divergence of both MICOS and ATPase in *T. brucei* (Montgomery et al., 2018). The exact roles of ATPase and TbMICOS have yet to be studied in regards to their dual functionality on cristae curvature.

The discovery of reduced levels of TbErv1 in three knockdown cell lines received greater interest. Until now, a functional homolog for Mia40 has yet to be identified in kinetoplastids (Haindrich et al., 2017). This central enzyme of the MIA pathway is distributed widely among the eukaryotes (Stojanovski et al., 2012; Munoz-Gomez et al., 2015b). The signature reaction of this pathway is the disulfide relay system between Mia40 and Erv1, as Erv1 binds to Mia40 to enable reoxidation of the latter, allowing the recycling of Mia40 for IMS import (Hell 2008). TbMic20 appears to have the capacity to fulfil this key role.

TbMic20 contains a thioredoxin-like domain, including a CIPC motif that may react with unfolded precursor proteins in the IMS through thiol-bridge formation, similar to the CPC reaction center in

Mia40 (Banci et al., 2009). Moreover, TbMic20 is shown to interact strongly with TbMICOS based on immunoblot analysis along its depletion of TbErv1 when silenced. The elongation of cristae due to TbMic20 knockdown further supports the protein's central role in the complex. This, along with cellular growth arrests in glucose-rich medium, points towards the theory that TbMICOS also performs a critical role in IMS import. The MIA pathway is not only involved in the importation of assembly factors for respiratory chain complexes embedded throughout cristae, but also in mitochondrial biogenesis itself (Wenger et al., 2017). Hence, it may be lightly suggested that growth arrest under the depletion of TbMICOS in the presences of a glucose-rich environment is the result of mitochondrial importation retardation.

Since the MIA pathway also shows similarities with oxidation systems found in bacterial periplasm, despite the lack of protein homology, it is considered that the Mia40-Erv1system contains endosymbiotic origins from bacteria (Hell 2008). This in of itself is exciting, since TbMic20 could very well have derived from the same thioredoxin-like proteins involved in disulfide introduction found in bacteria: DsbA and PDI (Collet & Bardwell 2008). Although Mia40 and TbMic20 lack structural and sequence similarity to both DsbA and PDI, the results presented here show that these proteins may indeed show analogous functions yet novel properties

In conclusion, this thesis represents a one of the first stepping stones in the investigation of MICOS outside opisthokonts. The characteristics of this multiprotein complex within excavates presented here pave the road in understanding the evolution of the mitochondria, a fundamental question that has puzzled many since the birth of modern day biology. These results unveil that MICOS indeed shows divergence, with the ability to adapt to facilitate different metabolic pathways, as seen in the case of TbMic20 and growth arrest in the presence of glucose. However, TbMICOS also shows evolutionary conserved core functions, such as the ability to achieve proper cristae morphology. This work opens a number of doors to questions that arise from these results: whether TbMic20 is indeed a functional analog of Mia40, if TbMICOS differs between the procyclic and bloodstream life cycles, and if ATPase and MICOS do play separate, yet antagonistic roles in membrane curvature and formation in *T. brucei*. Is the exploration of novelties in apparently 'conserved' mitochondrial proteins throughout all eukaryotes the key to understanding the exact origin of the mitochondria? With this, one must ask, what other surprises does MICOS have hidden throughout these eukaryotes?

7. Appendix

7.1. List of Abbreviations:

ATP	Adenosine Triphosphate
ATPase	ATP Synthase
bp	Base Pairs
CJ	Cristae Junction
Co-IP	Protein Complex Immunoprecipitation
dsRNA	Double-Stranded RNA
ERV1	Essential for Respiration and Vegetative Growth Protein 1
HA	Human Influenza Hemagglutinin
HEPES	N-2-Hydroxy Ethyl Piperazine N`-2-Ethane Sulfonic Acid
HSP70	70 kilo Dalton Heat Shock Proteins
lhRNA	Long Hairpin RNA
IMS	Mitochondrial Intermembrane Space
IP	Immunoprecipitation
LB	Lysogeny Broth
LDS	Lithium Dodecyl Sulfate
LDS-PAGE	Lithium Dodecyl Sulfate-Polyacrylamide Gel Electrophoresis
MES	2-(N-Morpholino) Ethane Sulfonic Acid
MIA	Mitochondrial IMS Import and Assembly
MICOS	Mitochondrial Contact Site and Cristae Organization System
MIM	Mitochondrial Inner Membrane
MOM	Mitochondrial Outer Membrane
NEB	New England Biolabs inc.
OXPHOS	Oxidative Phosphorylation
RISC	RNA-Induced Silencing Complex
RNAi	RNA Interference
PBS	Phosphate Buffered Saline
PCR	Polymerase Chain Reaction
SAM50	β-Barrel Sorting and Assembly Subunit
SOC	Super Optimal Broth
siRNA	Small Interfering RNA
ssRNA	Single-Stranded RNA
TAE	Tris-acetate-EDTA
Tb	*Trypanosoma brucei*
TEM	Transmission Electron Microscopy
TOM	Translocase of the Outer Membrane
VDAC	Voltage-Dependent Anion Channel

7.2. Primer Sequences:

Protein (Gene ID)	Forward Primer Sequence	Reverse Primer Sequence	Source
Tb927.9.10160	5'-acaagtttgtacaaaaaagcaggctaagcttCTCAAGGCTTTTGTGGCTTC-3'	5'-accactttgtacaagaaagctgggtctcgagATGGGTCTTTCCACACCGTA-3'	Sigma Aldrich
Tb927.11.6470	5'-acaagtttgtacaaaaaagcaggctaagcttAGCCTCAAGGACTGTGGTGT-3'	5'-accactttgtacaagaaagctgggtctcgagAATCATCCTCGATGTCTGCC-3'	Sigma Aldrich
Tb927.5.690	5'-acaagtttgtacaaaaaagcaggctaagcttTGCGTCTAAAGGCACTGATG-3'	5'-accactttgtacaagaaagctgggtctcgagTCATATATCACCACCCGCTG-3'	Sigma Aldrich
Tb927.4.630	5'-acaagtttgtacaaaaaagcaggctaagcttCGAAGGAGGAGAGTTATGCG-3'	5'-accactttgtacaagaaagctgggtctcgagGCATGGTTGGGCTTAGTGAT-3'	Sigma Aldrich
Tb927.2.2940	5'-acaagtttgtacaaaaaagcaggctaagcttCACCCGCCGATAAGTTAGAA-3'	5'-accactttgtacaagaaagctgggtctcgagCTGGTCCGATTTCAGGTGTT-3'	Sigma Aldrich
Tb927.10.11900	5'-acaagtttgtacaaaaaagcaggctaagcttCCTTAGCGGTAGCGAGTACG-3'	5'-accactttgtacaagaaagctgggtctcgagTCATTAGCTCCTCCGCACTT-3'	Sigma Aldrich
Tb927.8.580	5'-acaagtttgtacaaaaaagcaggctaagcttTTCACAATTTTGCGCTTCTG-3'	5'-accactttgtacaagaaagctgggtctcgagACAGACATGTTGACGCTTGC-3'	Sigma Aldrich
Tb927.3.4380	5'-acaagtttgtacaaaaaagcaggctaagcttCAGCGTAGGCTCCTCGTATC-3'	5'-accactttgtacaagaaagctgggtctcgagACGGACCAACACTCCTGAAC-3'	Sigma Aldrich
pTrypSon	5'-CGCTGACTTTCCAAGACCTC-3'	5'-CAGATCGTCTTCACCCCCTA-3'	Sigma Aldrich

8. References

Adl, S. *et al*. The revised classification of eukaryotes. *The Journal of Eukaryotic Microbiology* 59, 429–493 (2012).

Anselmi, C., Davies, K. M. & Faraldo-Gomez, J. D. Mitochondrial ATP synthase dimers spontaneously self-associate driven by a long-ranged membrane-induced force. (2018).

Atayde, V. D., Ullu, E. & Kolev, N. G. A single-cloning-step procedure for the generation of RNAi plasmids producing long stem–loop RNA. *Molecular and Biochemical Parasitology* 184,55–58 (2012).

Banci, L. *et al.* MIA40 is an oxidoreductase that catalyzes oxidative protein folding in mitochondria. *Nature Structural & Molecular Biology* 16, 198–206 (2009).

Basu, S. *et al*. Divergence of Erv1-Associated Mitochondrial Import and Export Pathways in Trypanosomes and Anaerobic Protists. *Eukaryotic Cell* 12, 343–355 (2012).

Bohnert, M. et al. Central Role of Mic10 in the Mitochondrial Contact Site and Cristae Organizing System. *Cell Metabolism* 21, 747–755 (2015).

Collet, J.-F. & Bardwell, J. C. Disulfide Bond Formation in Prokaryotes. *Protein Science Encyclopedia* (2008).

Coustou, V. *et al.*Glucose-induced Remodeling of Intermediary and Energy Metabolism in Procyclic Trypanosoma brucei. *Journal of Biological Chemistry* 283, (2008).

Davies, K. & Kühlbrandt, W. Structure of the catalytic F1 head of the F1-Fo ATP synthase from Trypanosoma brucei. *Proceedings of the National Academy of Sciences of the United States of America* (2018).

Davies, K. M., Anselmi, C., Wittig, I., Faraldo-Gomez, J. D. & Kühlbrandt, W. Structure of the yeast F1Fo-ATP synthase dimer and its role in shaping the mitochondrial cristae. *Proceedings of the National Academy of Sciences of the United States of America* 109, (2012).

Eckers, E. *et al.*Divergent Molecular Evolution of the Mitochondrial Sulfhydryl: Cytochromec Oxidoreductase Erv in Opisthokonts and Parasitic Protists. *Journal of Biological Chemistry* 288, 2676–2688 (2012).

Fire, A. et al. Potent and specific genetic interference by double-stranded RNA in Caenorhabditis elegans. *Nature* 309, 806–811 (1998).

Friedman, J. R., Mourier, A., Yamada, J., Mccaffery, J. M. & Nunnari, J. MICOS coordinates with respiratory complexes and lipids to establish mitochondrial inner membrane architecture. *eLife* 4,(2015).

Gibson, D. et al. One-step enzymatic assembly of DNA molecules up to several hundred kilobases in size. *Nature Methods* (2009).

Gossen, M. *et al.*Transcriptional activation by tetracyclines in mammalian cells. *Science* 268,1766–1769 (1995).

Haindrich, A. C. et al. The intermembrane space protein Erv1 of Trypanosoma brucei is essential for mitochondrial Fe-S cluster assembly and operates alone. *Molecular and Biochemical Parasitology* 214, 47–51 (2017).

Hampl, V. et al. Phylogenomic analyses support the monophyly of Excavata and resolve relationships among eukaryotic "supergroups". *Proceedings of the National Academy of Sciences of the United States of America* 106, 3859–3864 (2009).

Harner, M. *et al.*The mitochondrial contact site complex, a determinant of mitochondrial architecture. *The EMBO Journal* 30,4356–4370 (2011).

Hell, K. The Erv1–Mia40 disulfide relay system in the intermembrane space of mitochondria. *Biochimica et Biophysica Acta (BBA) - Molecular Cell Research* 1783, 601–609 (2008).

Herrmann, J. M. MINOS Is Plus: A Mitofilin Complex for Mitochondrial Membrane Contacts. *Developmental Cell* 21,599–600 (2011).

Hohr, A. *et al* Membrane protein insertion through a mitochondrial β-barrel gate. *Science* 359, (2018).

Hoppins, S. *et al* A mitochondrial-focused genetic interaction map reveals a scaffold-like complex required for inner membrane organization in mitochondria. *Journal of Cell Biology* 323–340 (2011).

Horvath, S. *et al.*Role of membrane contact sites in protein import into mitochondria. *Protein Science* 277–297 (2015).

Huynen, M. A., Mühlmeister, M., Gotthardt, K., Guerrero-Castillo, S. & Brandt, U. Evolution and structural organization of the mitochondrial contact site (MICOS) complex and the mitochondrial intermembrane space bridging (MIB) complex. *Biochimica et Biophysica Acta (BBA) - Molecular Cell Research* 1863, 91–101 (2016).

Jakob, M. Mitochondrial growth during the cell cycle of Trypanosoma brucei bloodstream forms. *Scientific Reports* 6 ,(2016).

Kalidas, S., Li, Q. & Phillips, M. A. A Gateway® compatible vector for gene silencing in bloodstream form Trypanosoma brucei. *Molecular and Biochemical Parasitology* 178 **,**51–55 (2011).

Korner, C. et al. The C-terminal domain of Fcj1 is required for formation of crista junctions and interacts with the TOB/SAM complex in mitochondria. *Molecular Biology of the Cell* 23, 2143–2155 (2012).

Kozjak-Pavlovic, V. The MICOS complex of human mitochondria. *Cell and Tissue Research* 367, 83–93 (2016).

Matthews, K. R. The developmental cell biology of Trypanosoma brucei. *Journal of Cell Science* 118, 283–290 (2005).

Mcallaster, M. R., Sinclair-Davis, A. N., Hilton, N. A. & Graffenried, C. L. D. A unified approach towards Trypanosoma brucei functional genomics using Gibson assembly. *Molecular and Biochemical Parasitology* 210, 13–21 (2016).

Montgomery, M. G., Gahura, O., Leslie, A. G. W., Zíková, A. & Walker, J. E. ATP synthase from Trypanosoma bruceihas an elaborated canonical F1-domain and conventional catalytic sites. *Proceedings of the National Academy of Sciences* 115,2102–2107 (2018).

Muñoz-Gómez, S. A. et al. Ancient homology of the mitochondrial contact site and cristae organizing system points to an endosymbiotic origin of mitochondrial cristae. *Current Biology* 25, (2015a).
Muñoz-Gómez, S. A., Slamovits, C. H., Dacks, J. B. & Wideman, J. G. The evolution of MICOS: Ancestral and derived functions and interactions. *Communicative & Integrative Biology* 8, (2015b).

Ngo, H., Tschudi, C., Gull, K. & Ullu, E. Double-stranded RNA induces mRNA degradation in Trypanosoma brucei. *Proceedings of the National Academy of Sciences* 95, 14687–14692 (1998).

Ott, C., Dorsch, E., Fraunholz, M., Straub, S. & Kozjak-Pavlovic, V. Detailed Analysis of the Human Mitochondrial Contact Site Complex Indicate a Hierarchy of Subunits. *Plos One* 10, (2015).

Paddison, P. J., Caudy, A. A., Bernstein, E., Hannon, G. J. & Conklin, D. S. Short hairpin RNAs (shRNAs) induce sequence-specific silencing in mammalian cells. *Genes & Development* 16, 948–958 (2002).

Pfanner, N. et al. Uniform nomenclature for the mitochondrial contact site and cristae organizing system. *Journal of Cell Biology* 204, 1083–1086 (2014).

Poon, S. K., Peacock, L., Gibson, W., Gull, K. & Kelly, S. A modular and optimized single marker system for generating Trypanosoma brucei cell lines expressing T7 RNA polymerase and the tetracycline repressor. *Open Biology* 2, 110037–110037 (2012).

Rabl, R. *et al*. Formation of cristae and crista junctions in mitochondria depends on antagonism between Fcj1 and Sue/g. *The Journal of Cell Biology* 185**,**1047–1063 (2009).

Rampelt, H., Zerbes, R. M., van der Laan, M. & Pfanner, N. Role of the mitochondrial contact site and cristae organizing system in membrane architecture and dynamics. *Biochimica et Biophysica Acta (BBA) - Molecular Cell Research* 1864, 737–746 (2017a).

Rampelt, H. *et al* .Mic10, a Core Subunit of the Mitochondrial Contact Site and Cristae Organizing System, Interacts with the Dimeric F 1 F o -ATP Synthase. *Journal of Molecular Biology* 429**,**1162–1170 (2017b).

Stojanovski, D., Bragoszewski, P. & Chacinska, A. The MIA pathway: A tight bond between protein transport and oxidative folding in mitochondria. *Biochimica et Biophysica Acta (BBA) - Molecular Cell Research* 1823, 1142–1150 (2012).

Tarasenko, D. et al. The MICOS component Mic60 displays a conserved membrane-bending activity that is necessary for normal cristae morphology. *The Journal of Cell Biology* 216, 889–899 (2017).

Ullu, E., Kolev, N., Barnes, R. & Tschudi, C. in *RNA Metabolism in Trypanosomes* (2012).

Varabyova, A. *et al*. Mia40 and MINOS act in parallel with Ccs1 in the biogenesis of mitochondrial Sod1. *The FEBS Journal* 280, (2013).

Vickerman, K. Polymorphism and Mitochondrial Activity In Sleeping Sickness Trypanosomes. *Nature* 208, 762–766 (1965).

Vickerman, K. Developmental Cycles And Biology Of Pathogenic Trypanosomes. *British Medical Bulletin* 41,105–114 (1985).

Vogel, F., Bornhövd, C., Neupert, W. & Reichert, A. S. Dynamic subcompartmentalization of the mitochondrial inner membrane. *The Journal of Cell Biology* 175, 237–247 (2006).

von der Malsburg, K. *et al.* Dual role of mitofilin in mitochondrial membrane organization and protein biogenesis. *Developmental Cell* 18, 694-707 (2011)

Wang, Z., Morris, J. C., Drew, M. E. & Englund, P. T. Inhibition ofTrypanosoma brucei Gene Expression by RNA Interference Using an Integratable Vector with Opposing T7 Promoters. *Journal of Biological Chemistry* 275, 40174–40179 (2000).

Wenger, C., Oeljeklaus, S., Warscheid, B., Schneider, A. & Harsman, A. A trypanosomal orthologue of an intermembrane space chaperone has a non-canonical function in biogenesis of the single mitochondrial inner membrane protein translocase. *PLOS Pathogens* 13,(2017).

Wiedemann, N. & Pfanner, N. Mitochondrial Machineries for Protein Import and Assembly. *Annual Review of Biochemistry* 86, 685–714 (2017).

Wirtz, E. & Clayton, C. Inducible gene expression in trypanosomes mediated by a prokaryotic repressor. *Science* 268**,**1179–1183 (1995).

Wollweber, F., Malsburg, K. V. D. & Laan, M. V. D. Mitochondrial contact site and cristae organizing system: A central player in membrane shaping and crosstalk. *Biochimica et Biophysica Acta (BBA) - Molecular Cell Research* 1864, 1481–1489 (2017).

Zíková, A., Verner, Z., Nenarokova, A., Michels, P. A. M. & Lukeš, J. A paradigm shift: The mitoproteomes of procyclic and bloodstream Trypanosoma brucei are comparably complex. *PLOS Pathogens* 13, (2017).